7. Formulation, development and evaluation of CS encapsulated core-shell polymer-lipid hybrid nanoparticles (CS-PLHNs)

7.1 Experimental methods

7.1.1 Pre-formulation studies

The following preformulation studies were performed for successful development of CS-PLHNs.

7.1.1.1 Drug excipients compatibility studies

7.1.1.1.1 Fourier transform infrared (FTIR) spectroscopy

FTIR spectroscopic study of CS, PLGA, soya lecithin, PVA and their physical mixture was conducted using FTIR spectrophotometer (Shimadzu, Model-8400S, Japan) in order to assess the possibility of chemical interaction, if any, between CS and other excipients. The analysis was performed by following the same protocol as mentioned in ***sub-section 5.1.1.2.1.***

7.1.1.1.2 Differential scanning calorimetry (DSC) study

The thermal behaviour of CS, PLGA, soya lecithin, PVA and their physical mixture was characterized by using TGA/DSC-1, Star® system (Mettler Toledo, Switzerland) with an auto cool accessory, for evaluating the compatibility of CS with other excipients. The analysis was performed by following the same protocol as mentioned in ***sub-section 5.1.1.2.2.***

7.1.2 Formulation of CS encapsulated core-shell polymer-lipid hybrid nanoparticles

PLGA-soya lecithin based CS-PLHNs were engineered by double emulsification solvent evaporation ($W_1/O/W_2$) method with suitable modifications as earlier reported

by Patel *et al* [54]. In brief, 25 mg of CS was dissolved in 0.5 ml of DDW (W_1) while weighed amount of PLGA was dissolved in dichloromethane (O) containing span 80. The external aqueous phase (W_2) was prepared by dispersing designated amount of soya lecithin and PVA in DDW containing acetic acid (0.1 %v/v) and tetrahydrofuran (4 %v/v). The internal aqueous phase (W_1) was added in an organic phase (O) and emulsified with the help of ultra probe sonicator (UP50H, Hielscher, USA) for 90 sec at 80% sonication amplitude over an ice bath. The formed primary emulsion (W_1/O) was poured into the external aqueous phase (W_2) under continuous stirring and then whole mixture was sonicated over an ice bath, using ultra probe sonicator for 5 min at 80% sonication amplitude. The resultant double emulsion (W_1/O/W_2) was allowed to stirr magnetically at 1000 rpm for 6 hr at room temperature in order to evaporate residual DCM completely and to form CS-PLHNs. Subsequently, CS-PLHNs were concentrated by removing organic phase and excess water, under reduced pressure using rotatory evaporator (IKA® RV10, Germany). The resulting CS-PLHNs were recovered by centrifugation at 15,000 rpm using cooling centrifuge (RC 4100 F, Eltek, Mumbai, India) for 15 min at 4 ^{o}C temperature. The supernatant was separated and kept aside for drug content analysis as described later. The CS-PLHNs, gathered in the form of sediment were washed three times and then resuspended in a fixed volume of DDW. The CS-PLHNs were lyophilized with mannitol (2 %w/v) using freeze dryer (Labconco, USA) for 48 hr, at -45 ^{o}C and 0.050 mbar vacuum pressure. The lyophilized CS-PLHNs were stored in a desiccator at 4 ^{o}C until further use.

7.1.3 Experimental design

7.1.3.1 Preliminary screening of variables by using Plackett-Burman screening design

A set of experiments with Plackett–Burman statistical experimental design was performed to screen the effect of various formulation and process variables on the CQAs of CS-PLHNs [54, 177] as described in ***sub-section 5.1.3.1***. The Design Expert® software (Version 8.0.6.1, Stat-Ease Inc., Minneapolis, USA) was utilized for the generation of randomized design matrix and evaluation of statistical experimental design. Each variable was represented at two levels, namely, "high" and "low". These levels define the upper and lower limits of the range covered by each variable. The level selection of different variables was based on a preliminary study and findings in the existing scientific literature. Different 11 independent variables were tested at 12 experimental runs. The selected experimental variables along with their levels, used for the screening design are depicted in Table 7.1. The particle size (Y_1), EE (Y_2) and PDI (Y_3) of CS-PLHNs were selected as dependent variables (CQAs). Results of the different experimental runs were analyzed by employing multiple linear regressions using one-way ANOVA, in order to determine the significance of the selected model along with the factor coefficients. Results obtained were statistically analyzed at 5% level of significance [54, 178]. All experiments were performed in a triplicate and randomized order.

Table 7.1 Experimental variables with their levels in Plackett-Burman screening design.

Variables	Level	
Independent Variables	Low (-1)	High (+1)
A : Lipid/polymer ratio (w/w)	0.25	0.5
B : Concentration of external surfactant (%w/v)	0.3	0.6
C : Organic phase/aqueous phase ratio (v/v)	0.16	0.33
D : Concentration of polymer (%w/v)	1.5	3
E : Sonication time (min)	3	6
F : Sonication amplitude (%)	40	80
G : Types of organic phase	DCM	EA
H : Concentration of internal surfactant (%w/v)	0.05	0.1
I : Types of drug	CS	GAN
J : Stirring speed (rpm)	1000	1500
K : Stirring temp (^{o}C)	25	40

Where, DCM: Dichloromethane; EA: Ethyl acetate; CS: Cromolyn sodium; GAN: Ganciclovir

7.1.3.2 Optimization of variables by using Box-Behnken Experimental Design

The critical variables obtained after preliminary screening through the Plackett-Burman screening design, were applied to RSM for statistical optimization of the CS-PLHNs. In current study, a response surface method, 3-level, 4-factor, Box-Behnken experimental design with statistical model incorporating interactive and polynomial terms was utilised for optimization, quantification and establishing the relationship between the clusters of controlled independent variables and the physicochemical properties of CS-PLHNs [179-181], as described in ***sub-section 5.1.3.2***.

Based on initial screening in the preliminary studies, lipid/polymer ratio (X_1), concentration of surfactant (X_2), organic phase/aqueous phase ratio (X_3) and concentration of polymer (X_4) were opted as four critical independent variables. Each critically selected variable is varied at three different levels. Higher, middle and lower level of each variable is coded as +1, 0 and -1, respectively, which were determined from preliminary experimentation. Other variables, which were evaluated in the preliminary Plackett-Burman screening design, were adjusted to the fixed level in the Box-Behnken experimental design owing to their statistically insignificant effect on the dependent variables. The studied particle size (Y_1), EE (Y_2) and PDI (Y_3) of prepared CS-PLHNs were taken as dependent variables. All independent and dependent variables along with applied constraints, in the form of actual and coded levels are summarized in Table 7.2.

Table 7.2 Independent variables with their levels and dependent variables in Box-Behnken experimental design

Independent variables	**Coded levels of variables**		
	Low	**Medium**	**High**
	-1	0	1
X_1 = Lipid/polymer ratio (w/w)	0.25	0.38	0.5
X_2 = Concentration of surfactant (%w/v)	0.5	1	1.5
X_3 = Organic phase/aqueous phase ratio (v/v)	0.16	0.25	0.33
X_4 = Concentration of polymer (%w/v)	1.5	2.25	3.0
Dependent variables (Responses)	**Constraints**		
Y_1= Particle size (nm)	Minimize		
Y_2= Encapsulation efficiency (%)	Maximize		
Y_3= Polydispersity index (PDI)	Minimize		

The design matrix comprising of 29 runs, along with quadratic response surface and second order polynomial model was constructed by using Design-Expert software®

(8.0.6.1, Stat-Ease Inc., Minneapolis, USA). All experiments were run in a randomized order to avoid any possible source of experimental bias and to increase the predictability of the model.

Multiple linear regression was applied by employing the ANOVA, in order to ascertain the influence and significance of factors along with their interactive effect on the response variables. Numerical output of ANOVA was represented in terms of *p*-value and $p<0.05$ was considered as statistically significant. 3D response surface plots and second order polynomial models were generated to quantify the correlation between independent variables and dependent variables as well as to determine the design space [179-182].

After generating the polynomial equations for the respective dependent variables, desirability approach based numerical optimization technique was probed for optimizing the CS-PLHNs with desired quality traits. The different constraints for independent variables were set in order to obtain the levels of independent variables, which would yield optimized CS-PLHNs with maximum EE and minimum particle size with low PDI. Desirability function was probed for combining all the responses in one measurement in order to predict the optimum levels for the independent variables. By considering this fact, the optimization was performed through the software for obtaining the best preferable formulation. Subsequently, the experimentally optimized formulation was prepared and tested to verify the correlation between the actual and predicted responses and thereby, validity of the model [23, 45, 179, 183]. The optimized CS-PLHNs were further subjected to various characterizations, *in-vitro* and *in-vivo* evaluation studies.

7.1.4 Characterizations of CS-PLHNs

7.1.4.1 Particle size, polydispersity index (PDI) and zeta potential

Measurement of particle size, zeta potential and PDI of prepared CS-PLHNs was carried out by photon correlation spectroscopy using DELSA^{TM} NANO C particle size analyzer (Beckman Coulter, Inc., UK) at 25 ^{o}C temperature. The electrophoretic mobility of CS-PLHNs, under the influence of an applied electric field was measured for determination of zeta potential [184, 185]. Analysis was performed by following the same protocol as described in ***sub-section 5.1.4.1.***

7.1.4.2. Encapsulation efficiency (EE) and drug loading

The EE (%) and drug loading (%) of CS in prepared CS-PLHNs ware measured spectrophotometrically (Shimadzu UV 1800, Japan) at λ_{max} of 239 nm by estimating the free CS content in supernatant obtained after the centrifugation (indirect method) [29, 45]. Analysis was performed by following the same protocol as described in ***sub-section 5.1.4.2.***

7.1.4.3 Solid state characterizations

7.1.4.3.1 Fourier transform infrared spectroscopy (FTIR) study

The FTIR spectra of pure CS and optimized CS-PLHNs were recorded by following the same protocol and same instrument as mentioned in the ***sub-section 5.1.1.2.1*** in order to evaluate any significant change, if occurs, during the encapsulation of CS inside the matrix of polymer-lipid hybrid nanoparticles (PLHNs).

7.1.4.3.2 Differential scanning calorimetry (DSC) study

The physical state of CS inside PLHNs was assessed by DSC study. The DSC thermograms of pure CS and optimized CS-PLHNs were recorded by following the same protocol and same instrument as mentioned in the ***sub-section 5.1.1.2.2***.

7.1.4.3.3 Powder X-ray diffractometry (PXRD) study

The PXRD patterns of pure CS, PLGA, soya lecithin, PVA, physical mixture and optimized CS-PLHNs were obtained by following the same protocol and same instrument as mentioned in the ***sub-section 5.1.4.3.3*** in order to determine the change in the physical state of CS, if occurs during the encapsulation process.

7.1.4.4 Shape and surface morphology

7.1.4.4.1 High resolution transmission electron microscopy (HR-TEM)

The shape and surface morphology of the optimized CS-PLHNs was examined by following the same protocol and same instrument as mentioned in the ***sub-section 5.1.4.4.1.***

7.1.4.4.2 Atomic force microscopy (AFM)

The surface morphology of optimized CS-PLHNs was visualized by following the same protocol and same instrument as mentioned in the ***sub-section 5.1.4.4.2.***

7.1.4.4.3 Confocal laser scanning microscopy (CLSM)

The core-shell structure of CS-PLHNs was visualized by using confocal laser scanning microscope (LSM 510 META, Carl Zeiss Inc., USA). For this study, FITC tagged micron sized CS-PLHNs were intentionally prepared by using similar procedure, by eliminating the sonication step [141]. The fluorescent core was obtained by using the FITC tagged PLGA.

7.1.4.5 *In-vitro* drug release study

The *in-vitro* drug release study of optimized CS-PLHNs was performed using modified dialysis bag diffusion technique in phosphate buffer pH 7.4. The same protocol was followed for *in-vitro* drug release study and release kinetic modeling as mentioned in the ***sub-section 5.1.4.5.***

7.1.4.6 Accelerated and real time storage stability study

The stability of optimized CS-PLHNs was assessed over a period of 6 month at room temperature (25 $\pm$ 2 ^{o}C), refrigerated condition (4 $\pm$ 1 ^{o}C), and accelerated condition (40 $\pm$ 2 ^{o}C/75 $\pm$ 5 % RH) as per ICH guideline by following the same protocol as mentioned in the ***sub-section 5.1.4.6.***

7.1.4.7 Animal studies

7.1.4.7.1 Animals

The animal study protocol was duly approved by Central Animal Ethical Committee of Banaras Hindu University (No. Dean/2014/CAEC/856). The animal details are discussed earlier in ***sub-section 5.1.4.7.1.***

7.1.4.7.2 *Ex-vivo* intestinal permeation study

The intestinal permeation potential of CS-PLHNs across the GIT was assessed by *ex-vivo* intestinal permeation study using non-everted gut sac technique by following the same method as described in **s*ub-section 5.1.4.7.2.***

7.1.4.7.3 *In-vivo* intestinal uptake study

The intestinal particulate uptake and permeation of CS-PLHNs was visualized by CLSM upon oral administration of FITC labelled CS-PLHNs in rats. *In-vivo* intestinal

uptake study was performed by following the same method as described in ***sub-section 5.1.4.7.3.***

7.1.4.7.4 *In-vivo* pharmacokinetic study

7.1.4.7.4.1 *Dosing and sampling*

The same dosing and sampling protocol as described in **s*ub-section 5.1.4.7.4.1*** was followed for the determination of pharmacokinetic profile of CS-PLHNs after oral administration in the rats.

7.1.4.7.4.2 *Chromatography conditions and drug extraction*

The same in-house validated RP-HPLC method was followed for determination of CS concentration in blood plasma as described in ***sub-section 4.1.2*.** The details of chromatography conditions and drug extraction are mentioned in ***sub-section 4.1.2.1 and 4.1.2.4***, respectively.

7.1.4.7.4.3 *Pharmacokinetic parameters*

Various pharmacokinetic parameters for CS-PLHNs were determined as mentioned in ***sub-section 5.1.4.7.4.3*** using non-compartmental analysis of plasma drug concentration-time profile data through Winnonlin® 6.1 (Pharsight Corporation, Mountain View, CA) pharmacokinetic software.

7.1.4.7.5 *In-vivo* mast cell stabilizing activity

In-vivo mast cell stabilizing activity was studied by following the same protocol as mentioned in ***sub-section 5.1.4.7.5*** after oral administration of CS-PLHNs in rats.

7.1.4.8 Statistical analysis

The similar statistical analysis was performed using the GraphPad Prism software (version 5.03, GraphPad Software, USA) as mentioned in ***sub-section 5.1.4.8.*** The *p*-value less than 0.05 was considered as statistically significant.

7.2 Results and discussions

7.2.1 Pre-formulation studies

7.2.1.1 Drug excipients compatibility studies

7.2.1.1.1 Fourier transform infrared (FTIR) spectroscopy

FTIR study was performed for evaluating the compatibility between CS and components of PLHNs, which would be used for the preparation of CS-PLHNs. The FTIR spectra of CS, PLGA, soya lecithin, PVA and their physical mixture are depicted in Figure 7.1. The FTIR spectra of CS (Figure 7.1 (a)) exhibited two basic characteristic peaks at 1639.54 cm^{-1} and 3416 cm^{-1} indicative of C=O stretching and O-H stretching, respectively. The peaks at 2880 cm^{-1}, 1477 cm^{-1}, 1573 cm^{-1} and 1410 cm^{-1} are assigned to the alkane C-H, aromatic C-H, asymmetric and symmetric COO^{-}, respectively. Additionally, large number of characteristic absorption bands in fingerprint region (1400-600 cm^{-1}), were noticed as a result of vibration within the molecule [43, 45]. The FTIR spectra of PLGA (Figure 7.1 (b)) showed that the significant peaks of PLGA are C=O stretching at 1748.12 cm^{-1}, C-O stretching at 1194.25 cm^{-1}, C-H stretching at 2948.47 cm^{-1} and broad bands between 3200-3600 cm^{-1} due to its terminal hydroxyl group [205]. The FTIR spectra of soya lecithin showed characteristic band in the range of 1765-1720 cm^{-1} corresponding to the C=O vibration and another band in the range of 1200-1145 cm^{-1} due to the PO_2 vibration. Additionally, some characteristic bands in the range of 1200-970 cm^{-1} were noticed

corresponding to both P-O-C as well as PO_2 vibrations, respectively as shown in Figure 7.1 (c) [244]. In case of FTIR spectra of PVA (Figure 7.1 (d)), peaks in the range of 2840-3000 cm^{-1} for C-H stretching, 3200-3550 cm^{-1} for O-H stretching, 1290 cm^{-1} for C-N stretching and 1750-1735 cm^{-1} for C=O as well as C-O stretching from acetate group were observed [206]. All the major peaks pertaining to CS, PLGA, soya lecithin and PVA were retained in the FTIR spectra of physical mixture (Figure 7.1 (e)) at nearly same wavenumber as appeared in their single spectra, suggesting the non-involvement of CS in any kind of physicochemical interaction with the other excipients and prevalence of compatibility with the components of PLHNs [40, 23].

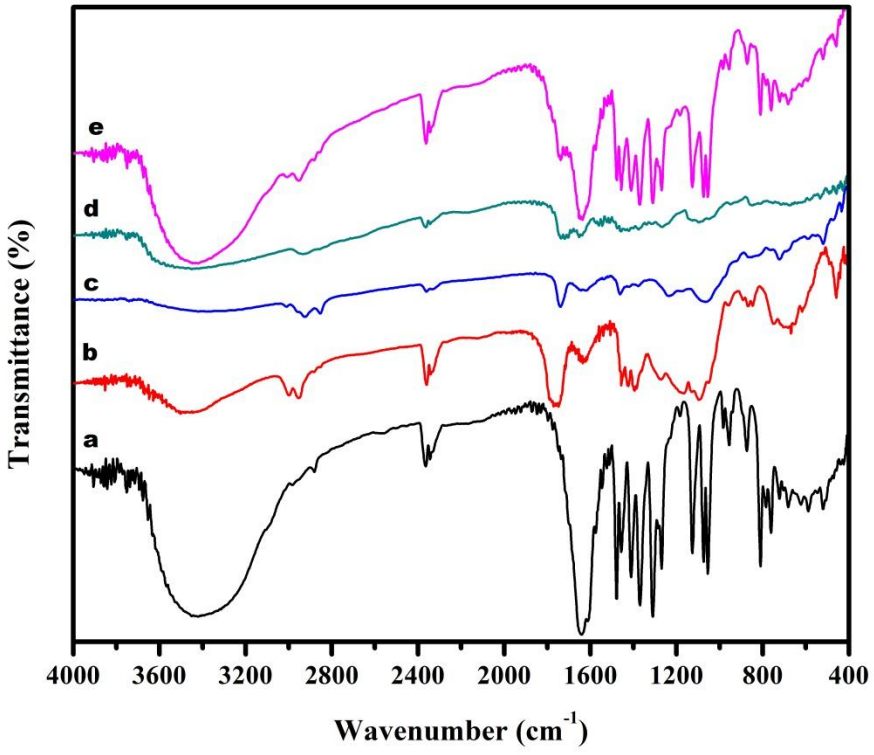

Figure 7.1 FTIR spectra of (a) CS, (b) PLGA, (c) soya lecithin, (d) PVA and (e) physical mixture

7.2.1.1.2 Differential scanning calorimetry (DSC) study

DSC thermograms of CS, PLGA, soya lecithin, PVA and their physical mixture are depicted in Figure 7.2. In the DSC thermogram of pure CS (Figure 7.2 (a)), sharp melting endotherm appeared at 264 ^{o}C attributed to its melting point, indicating its crystalline behaviour [149]. PLGA exhibited sharp endothermic peak at 65 ^{o}C (Figure 7.2 (b)). Soya lecithin displayed broad endothermic peak at 87 ^{o}C corresponding to its phase transition (Figure 7.2 (c)). PVA showed sharp endotherm at 226 ^{o}C corresponding to its melting point (Figure 7.2 (d)).

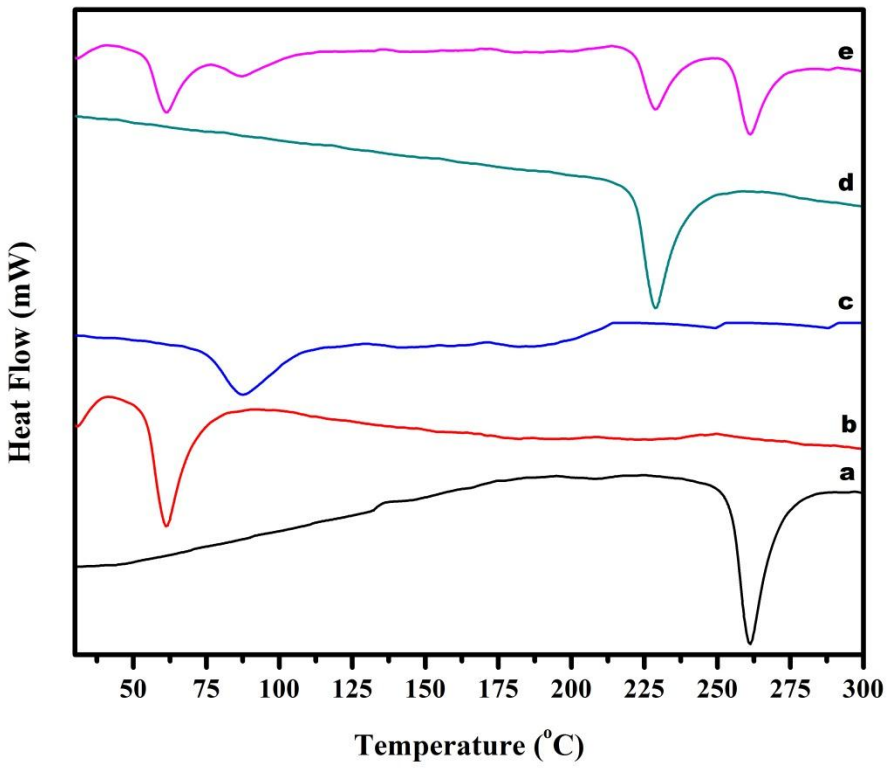

Figure 7.2 DSC thermograms of (a) CS, (b) PLGA, (c) soya lecithin, (d) PVA and (e) physical mixture

The thermogram of physical mixture of CS with the components of PLHNs also exhibited the similar thermal behaviour of CS at 264 ^{o}C as appeared in pure CS

thermogram. The physical mixture also showed the characteristic endothermic peaks of all the components of the PLHNs without any considerable shift in their peak positions, confirming the absence of interaction of CS with excipients. Moreover, no any new endothermic or degradation peak was observed in the thermogram of physical mixture (Figure 7.2 (e)), suggesting the existence of compatibility between CS and other excipients [23, 45, 207].

7.2.2 Experimental design

7.2.2.1 Preliminary screening of variables by using Plackett-Burman screening design

The physicochemical properties of CS-PLHNs prepared by double emulsification solvent evaporation ($W_1/O/W_2$) method are influenced by various formulation and process variables. The influence of various independent variables on the particle size, EE and PDI of the CS-PLHNs (CQAs) were studied by 11-factor, 2-level Plackett-Burman screening design. The Plackett–Burman statistical experimental design was employed for the initial screening and selection of critical variables affecting significantly to the formulation characteristics of CS-PLHNs, with good degree of accuracy during preliminary studies. It is a useful and efficient mathematical approach for evaluating the effect of large number of independent variables on particular CQAs by performing relatively few numbers of experimental runs. Based on literature search and existing scientific knowledge, various independent variables were selected as they are likely to affects the physicochemical properties of CS-PLHNs [54, 208, 209]. A total of 12 experimental trials, comprising of various combinations of different 11 independent variables were carried out as shown in Table 7.3.

Table 7.3 Plackett-Burman screening design experimental matrix

Run	A	B	C	D	E	F	G	H	I	J	K
1	0.5	0.6	0.16	3.00	6	80	DCM	0.05	CS	1500	25
2	0.25	0.6	0.33	1.50	6	80	EA	0.05	CS	1000	40
3	0.5	0.3	0.33	3.00	3	80	EA	0.1	CS	1500	25
4	0.25	0.6	0.16	3.00	6	40	EA	0.1	GAN	1500	25
5	0.25	0.3	0.33	1.50	6	80	DCM	0.1	GAN	1000	25
6	0.25	0.3	0.16	3.00	3	80	EA	0.05	GAN	1500	40
7	0.5	0.3	0.16	1.50	6	40	EA	0.1	CS	1000	40
8	0.5	0.6	0.16	1.50	3	80	DCM	0.1	GAN	1000	40
9	0.5	0.6	0.33	1.50	3	40	EA	0.05	GAN	1000	25
10	0.25	0.6	0.33	3.00	3	40	DCM	0.1	CS	1500	40
11	0.5	0.3	0.33	3.00	6	40	DCM	0.05	GAN	1500	40
12	0.25	0.3	0.16	1.50	3.00	40.00	DCM	0.05	CS	1000	25.00

Where, DCM: Dichloromethane; EA: Ethyl acetate; CS: Cromolyn sodium; GAN: Ganciclovir

Since Plackett-Burman screening designs are resolution 4 designs, only main effects of the selected independent variables were analyzed. The wide variation was observed in the selected dependent variables of CS-PLHNs, indicating that the independent variables had a significant effect on the response parameters chosen. Table 7.4 shows the results of different experimental runs in terms of different dependent variables.

Table 7.4 Results of dependent variables obtained through Plackett-Burman design.

Run	Particle Size (nm)	EE (%)	PDI
1	272 ± 7.4	85.5 ± 0.8	0.216 ± 0.022
2	131 ± 3.6	65.4 ± 3.4	0.161 ± 0.018
3	293 ± 1.1	92 ± 0.3	0.425 ± 0.089
4	152 ± 5.2	68.3 ± 5.4	0.192 ± 0.034
5	176 ± 4.9	72.5 ± 2.3	0.271 ± 0.017
6	225 ± 2.1	80.2 ± 3.6	0.242 ± 0.039
7	298 ± 3.7	88.1 ± 0.6	0.412 ± 0.048
8	261 ± 2.8	84.6 ± 1.1	0.296 ± 0.071
9	236 ± 1.4	81.4 ± 1.2	0.259 ± 0.026
10	178 ± 9.6	73 ± 3.5	0.124 ± 0.012
11	272 ± 2.3	86.2 ± 1.9	0.286 ± 0.051
12	192 ± 0.8	76.7 ± 1.7	0.298 ± 0.021

All values reported are mean ± SD; n = 3

Pareto chart showing the relative effect of the each independent variable on each dependent variable is depicted in Figure 7.3. It indicates the effect of independent variables plotted against the vertical axis as per their respective rank order. The

variables for which vertical bars extending passed the horizontal line suggested the statistical significance on the dependent variable [54, 210, 211].

Statistical analysis revealed that the particle size (Y_1) of the CS-PLHNs was significantly (p<0.05) influenced by four independent variables, i.e., lipid/polymer ratio (A), concentration of surfactant (B), organic phase/aqueous phase ratio (C) and concentration of surfactant (D), as indicated in Figure 7.3 (A) and Table 7.5. The value of correlation coefficient (R^2) was found to be 0.9865, indicating the goodness of fit of the model being tested. The *p*-value for the regression model was found to be 0.0002 and was considered as significant. All other independent variables showed non-significant (p>0.05) impact on the particle size. The model fitting values for different dependent variables, which indicate model adequacy are listed in Table 7.6.

For EE (Y_2) of the CS-PLHNs, the five most significant (p<0.05) independent variables were lipid/polymer ratio (A), concentration of surfactant (B), organic phase/aqueous phase ratio (C), concentration of polymer (D) and sonication time (E) amongst all other independent variables selected, as depicted in Figure 7.3 (B) and Table 7.5. The R^2 value for the regression model was 0.9978, indicating the goodness of fit of the model being tested. The *p*-value for the regression model was found to be significant (p=0.0007), confirming the adequate fitting to the model. All other independent variables also affected EE but their impact was statistically non-significant (p>0.05).

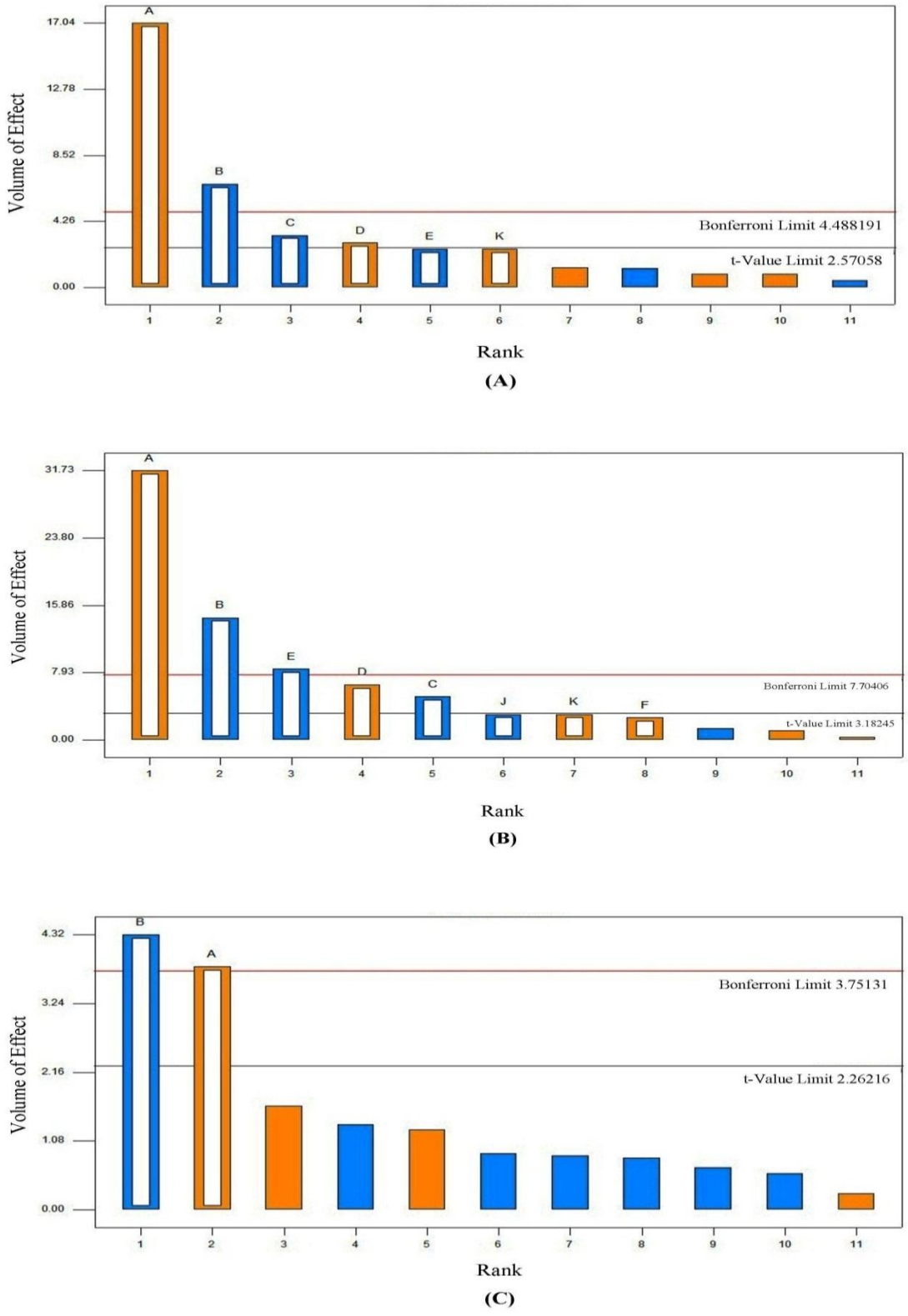

Figure 7.3 Pareto charts showing the significant effect of independent variables on (A) particle size, (B) EE and (C) PDI of CS-PLHNs during Plackett-Burman screening design

Table 7.5 Statistical analysis of dependent variables of Plackett-Burman screening design

Factor	Y_1 = Particle size		Y_2 = EE		Y_3 = PDI	
	Coefficient	***p* Value**	**Coefficient**	***p* Value**	**Coefficient**	***p* Value**
A	48.17	<0.0001	6.83	<0.0001	0.051	0.0041
B	-18.83	0.0012	-3.10	0.0007	-0.057	0.0019
C	-9.50	0.0201	-1.10	0.0145	-0.011	0.2175
D	8.17	0.0343	1.40	0.0074	-0.018	0.1427
E	-7.00	0.0561	-1.80	0.0036	-0.008	0.2674
F	2.50	0.3384	0.57	0.0783	0.003	0.1000
G	-1.33	0.1000	-0.28	0.2405	0.017	0.1247
H	2.50	0.3119	0.23	0.1772	0.021	0.1059
I	-3.50	0.2070	-0.65	0.0569	-0.007	0.2662
J	7.00	0.0561	0.65	0.0569	-0.011	0.2403
K	3.67	0.2276	0.067	0.1000	-0.012	0.2424

Whereas, PDI of the CS-PLHNs was found to be most significantly (p<0.05) dependent on the lipid/polymer ratio (A) and concentration of surfactant (B) relative to other variables, as observed in Figure 7.3 (C) and Table 7.5. The R^2 value for the regression model was found to be 0.7869, suggesting the significant goodness of fit of the model. The significant p-value (p=0.0010) for the regression model confirmed the adequate fitting to the model. All other independent variables showed non-significant (p>0.05) impact on the PDI. Thus, on the basis of results of the Plackett–Burman screening design, all the significantly affected independent variables on the

physicochemical attributes of CS-PLHNs were further evaluated by RSM for statistical optimization [54, 209, 210].

Table 7.6 Model summary statistics of the quadratic response surface models.

Response Variable	Model						
	F-value	**Prob>F***	**R^2**	**Adj. R^2**	**Pred. R^2**	**Adeq. Prec.**	**C.V. (%)**
Y_1	61.08	0.0002	0.9865	0.9704	0.9225	22.324	4.38
Y_2	172.13	0.0007	0.9978	0.9920	0.9652	40.652	0.94
Y_3	16.62	0.0010	0.7869	0.7395	0.6211	9.396	17.29

*Adj. R^2: Adjusted R^2; Pred. R^2: Predicted R^2; Adeq. Prec.: Adequate Precision; C.V.: Coefficient of Variation; *Prob>F is the significance level and a value less than 0.05 considered significant.*

7.2.2.2 Formulation optimization of variables by using Box-Behnken experimental design

According to the results obtained from the Plackett-Burman screening design, the total of four independent variables, namely lipid/polymer ratio, concentration of surfactant, organic phase/aqueous phase ratio and concentration of polymer were selected as critical variables for the statistical optimization of the CS-PLHNs using RSM [23, 210]. As the particle size and EE are more important for oral delivery of nanoparticles based on scientific literature, all common four independent variables were considered for systemic optimization. Whereas, other independent variables, which have affected significantly on the single dependent variables, were fixed to their higher or lower level corresponding to their negative or positive effect, respectively. A 3-level, 4-factor Box-Behnken experimental design based RSM was performed for precisely exploring and optimizing the influence of four independent variables i.e. lipid/polymer ratio (X_1), concentration of surfactant (X_2), organic

phase/aqueous phase ratio (X_3) and concentration of polymer (X_4) on dependent variables such as particle size (Y_1), EE (Y_2) and PDI (Y_3) of CS-PLHNs. A total of 29 batches of CS-PLHNs including 5 center points, were prepared as per design matrix generated by Box-Behnken experimental design by varying the four independent variables for all possible combinations. All the other independent variables used in the Plackett-Burman screening design, were found to have statistically non-significant effect on the physicochemical properties of CS-PLHNs in the selected range and hence, set to fix level during optimization using RSM [209, 210]. The statistical treatment combinations of the different independent variables along with the measured response variables obtained by performing experiments are summarized in Table 7.7.

Regression models and polynomial equations explaining the main effect, interactive effect as well as quadratic effect of the various independent variables on dependent variables were generated by fitting the results of the experimental design with the help of Design-Expert software®. Statistical significance of the selected model and the regression coefficients were estimated by multiple regressions using ANOVA. All the response variables were fitted to different regression models. For each response, the model which generated a higher F value was selected as the best fitted model. The accuracy and adequacy of the model was determined by measuring the R^2 value, which indicates the 'goodness of fit' of the model to the experimental results. The positive coefficient in polynomial equation suggests that the response varies directly with successive increase in the value of independent variables (i.e., synergistic effect), whereas the negative sign indicates that the response decreases with successive increase the value of independent variables (i.e., inverse effect). The absolute value of

the co-efficient indicates the magnitude of effect of the independent variables on the response variable; the higher the value the higher the magnitude [179, 211-213].

Table 7.7 Box-Behnken experimental design showing experimental runs with independent variables and their measured responses: particle size (Y_1), encapsulation efficiency (Y_2), and PDI (Y_3) of CS-PLHNs.

Run No.	Independent variables				Dependent variables		
	X_1	X_2	X_3	X_4	Y_1	Y_2	Y_3
Factorial Points							
1	-1	-1	0	0	281.1 ± 4.1	54.6 ± 0.8	0.257 ± 0.012
2	1	-1	0	0	339 ± 3.6	63.4 ± 0.2	0.386 ± 0.059
3	-1	1	0	0	249.1 ± 2.9	51.3 ± 2.4	0.176 ± 0.037
4	1	1	0	0	301 ± 2.1	59.1 ± 1.2	0.313 ± 0.061
5	0	0	-1	-1	283.4 ± 1.2	55.7 ± 3.7	0.265 ± 0.095
6	0	0	1	-1	257.1 ± 4.7	54.2 ± 0.7	0.230 ± 0.053
7	0	0	-1	1	310.8 ± 6.8	60.2 ± 0.5	0.300 ± 0.12
8	0	0	1	1	293.1 ± 7.3	57.8 ± 2.3	0.289 ± 0.038
9	-1	0	0	-1	268.5 ± 5.9	53.4± 1.9	0.218 ± 0.092
10	1	0	0	-1	313.9 ± 4.1	61.1 ± 0.1	0.331 ± 0.012
11	-1	0	0	1	284 ± 4.4	55.8 ± 2.9	0.269± 0.11
12	1	0	0	1	342.2 ± 11.2	63.6 ± 1.6	0.389 ± 0.024
13	0	-1	-1	0	316.3 ± 8.4	61.5 ± 0.3	0.342 ± 0.21
14	0	1	-1	0	257.6 ± 7.2	53 ± 0.9	0.195 ± 0.075
15	0	-1	1	0	294.1 ± 5.7	58.4 ± 1.6	0.302 ± 0.063
16	0	1	1	0	264.8 ± 3.8	53.3 ± 1.1	0.224 ± 0.01
17	-1	0	-1	0	263.1 ± 2.7	53.2 ± 2.4	0.221 ± 0.084
18	1	0	-1	0	334.6 ± 9.3	62.9 ± 1.1	0.378 ± 0.14
19	-1	0	1	0	261.4 ± 1.7	52.9 ± 3.7	0.209 ± 0.081
20	1	0	1	0	316.7 ± 4.8	61.6 ± 2.0	0.348 ± 0.096
21	0	-1	0	-1	286.1 ± 7.1	55.9 ± 0.5	0.261 ± 0.047
22	0	1	0	-1	268.8 ± 5.9	53.7 ± 0.8	0.230 ± 0.065
23	0	-1	0	1	321.9 ± 7.2	62 ± 2.1	0.362 ± 0.01
24	0	1	0	1	250.3 ± 2.6	51.8 ± 3.2	0.181 ± 0.013
Centre Points							
25	0	0	0	0	222.1 ± 4.6	58.7 ± 1.1	0.149 ± 0.043
26	0	0	0	0	216.3 ± 2.4	59.1 ± 1.9	0.141 ± 0.099
27	0	0	0	0	218.4 ± 6.3	60.5 ± 0.2	0.143 ± 0.12
28	0	0	0	0	221 ± 5.8	59.8 ± 2.1	0.145 ± 0.071
29	0	0	0	0	225 ± 3.9	60.8 ± 0.7	0.157 ± 0.032

All data are shown as mean ±S.D; n=3.

The mathematical relationships of independent variables' coefficients along with corresponding *p*-values for the dependent variables obtained by regression analysis are summarized in Table 7.8. *p*-value less than 0.05 was considered as statistically significance.

Table 7.8 Statistical analysis of dependent variables of Box-Behnken experimental design along with estimated regression coefficients and associated *p* values

Factor	Y_1 = Particle size		Y_2 = EE		Y_3 = PDI	
	Coefficient	***p* Value**	**Coefficient**	***p* Value**	**Coefficient**	***p* Value**
Intercept	220.56	< 0.0001	59.78	< 0.0001	0.15	< 0.0001
X_1	28.35	< 0.0001	4.21	< 0.0001	0.066	< 0.0001
X_2	-20.58	< 0.0001	-2.80	< 0.0001	-0.049	< 0.0001
X_3	-6.55	0.0052	-0.69	0.0342	-0.0082	0.0469
X_4	10.38	0.0001	1.43	0.0002	0.021	< 0.0001
X_1X_2	-1.50	0.6690	-0.25	0.6295	0.0020	0.7648
X_1X_3	-4.05	0.2580	-0.25	0.6295	-0.0045	0.5037
X_1X_4	3.20	0.3673	0.025	0.9614	0.0017	0.7934
X_2X_3	7.35	0.0504	0.85	0.1157	0.017	0.0197
X_2X_4	-13.57	0.0014	-2.00	0.0015	-0.037	< 0.0001
X_3X_4	2.15	0.5414	-0.24	0.6431	0.006	0.3756
X_1^2	44.09	< 0.0001	-0.38	0.3559	0.085	< 0.0001
X_2^2	28.53	< 0.0001	-2.24	< 0.0001	0.052	< 0.0001
X_3^2	31.39	< 0.0001	-1.40	0.0035	0.061	< 0.0001
X_4^2	34.78	< 0.0001	-1.34	0.0047	0.064	< 0.0001

3D response surface plots were constructed using respective polynomial equations to reveal the interactive effect of any two independent variables on dependent variable graphically, keeping third one at a constant level. The relationships between the dependent variable and the independent variables were also visualized by 2D contour plots for understanding the relative influence of the independent variable along with in combinations [179, 180, 182].

7.2.2.2.1 Influence of Independent variables on particle size

The particle size of the prepared CS-PLHNs was obtained from minimum of 216.3 $\pm$ 2.4 nm to maximum of 342.2 $\pm$ 11.2 nm for various independent variable level combinations in their limits, as per design matrix. The observed wide variation in response variable indicates that the particle size was strongly affected by the selected formulation variables. The quadratic model was selected for the statistical analysis of influence of independent variables on particle size based on the lack of fit test as shown in Table 7.9. The second-order, quadratic polynomial equation quantifying an empirical relationship between particle size (Y_1) and independent variables, generated by multiple linear regressions can be given as follows in terms of coded variables:

$$Y_1 = 220.56 + 28.35X_1 - 20.58X_2 - 6.55X_3 + 10.38X_4 - 13.57X_2X_4 + 44.09X_1^2 + 28.53X_2^2 + 31.39X_3^2 + 34.78X_4^2 \quad \text{Eq (7.1)}$$

Non-significant lack of fit value (p=0.0581; p>0.05) with F-value of 5.46 indicated that quadratic model is best fit to the independent variables for significantly describing the effect on the particle size. The high R^2 value (0.9832) implied the existence of reasonable agreement between predicted and experimental values for explaining the 98.32% variation in particle size. The minimal difference between predicted R^2 (0.9080) and adjusted R^2 (0.9664) value suggested the adequacy of the

selected model for the prediction of response. The value of adequate precision was found to be 24.907 (greater than 4 is desirable), suggesting an adequate signal to measure the signal independent of noise. Further, low value for coefficient of variation (2.47 %) indicated high degree of precision and reliability of the model. Hence, this selected quadratic model can be used to navigate the design space [23, 54, 179, 212].

Table 7.9 Statistical analysis results of lack of fit for particle size, EE and PDI of CS-PLHNs

Source	Sum of Squares	df	Mean Square	F Value	p-value Prob > F	
Particle size						
Linear	22727.02	20	1136.35	100.80	0.0002	-
2FI	21639.75	14	1545.70	137.11	0.0001	-
Quadratic	615.46	10	61.55	5.46	0.0581	Suggested
Cubic	97.39	2	48.70	4.32	0.1002	Aliased
Pure Error	45.09	4	11.27	-	-	-
Encapsulation efficiency						
Linear	74.40	20	3.72	4.67	0.0726	-
2FI	54.78	14	3.91	4.91	0.0679	-
Quadratic	11.20	10	1.12	1.40	0.3977	Suggested
Cubic	2.37	2	1.18	1.48	0.3296	Aliased
Pure Error	3.19	4	0.80	-	-	-
PDI						
Linear	0.085	20	0.00426	106.56	0.0002	-
2FI	0.078	14	0.00558	139.61	0.0001	-
Quadratic	0.002247	10	0.00022	5.62	0.0554	Suggested
Cubic	0.000416	2	0.00020	5.20	0.0771	Aliased
Pure Error	0.00016	4	0.00004	-	-	-

Statistical analysis revealed that lipid/polymer ratio (X_1) and concentration of polymer (X_4) affects positively, whereas concentration of surfactant (X_2) and organic phase/aqueous phase ratio (X_3) provides negative effect on particle size. Also higher coefficient value (28.35) of lipid/polymer ratio (X_1) suggested that it had most significant effect on particle size followed by concentration of surfactant (X_2), concentration of polymer (X_4) and organic phase/aqueous phase ratio (X_3). While in case of the interaction effects between different independent variables, only concentration of surfactant and concentration of polymer (X_2X_4) had combined significant effect on particle size. It is visually discerned from 3D response surface plots and 2D contour plots as displayed Figure 7.4.

The lipid/polymer ratio (X_1) appeared to be one of the most dominant variables amongst all, which positively influences particle size of CS-PLHNs owing to its direct effect on viscosity. The significant increment in particle size at higher lipid/polymer ratio could be attributed to the reduction of the shearing efficiency of stirrer at higher viscosity, which resulted in thick covering of the polymeric core by lipid coat. Additionally, higher lipid/polymer ratio also favors the formation of multilamellar liposomes due to the presence of high amount of lipid, above its critical micellar concentration and therefore, coexistence of liposomes with PLHNs might be responsible for measuring the larger particle size [50, 54]. Contrary, concentration of surfactant (X_2) holds inverse relationship with the particle size of CS-PLHNs. The remarkable drop off in the particle size was noticed at higher surfactant concentration, which might be due to reduction of the interfacial tension between the dispersed phase and dispersion medium [245]. Moreover, high surfactant concentration also offers droplet stabilization against coalescence during the emulsification process by

interfacial localization and thus, protects from impinging with each other in order to grow into bigger ones [215, 246].

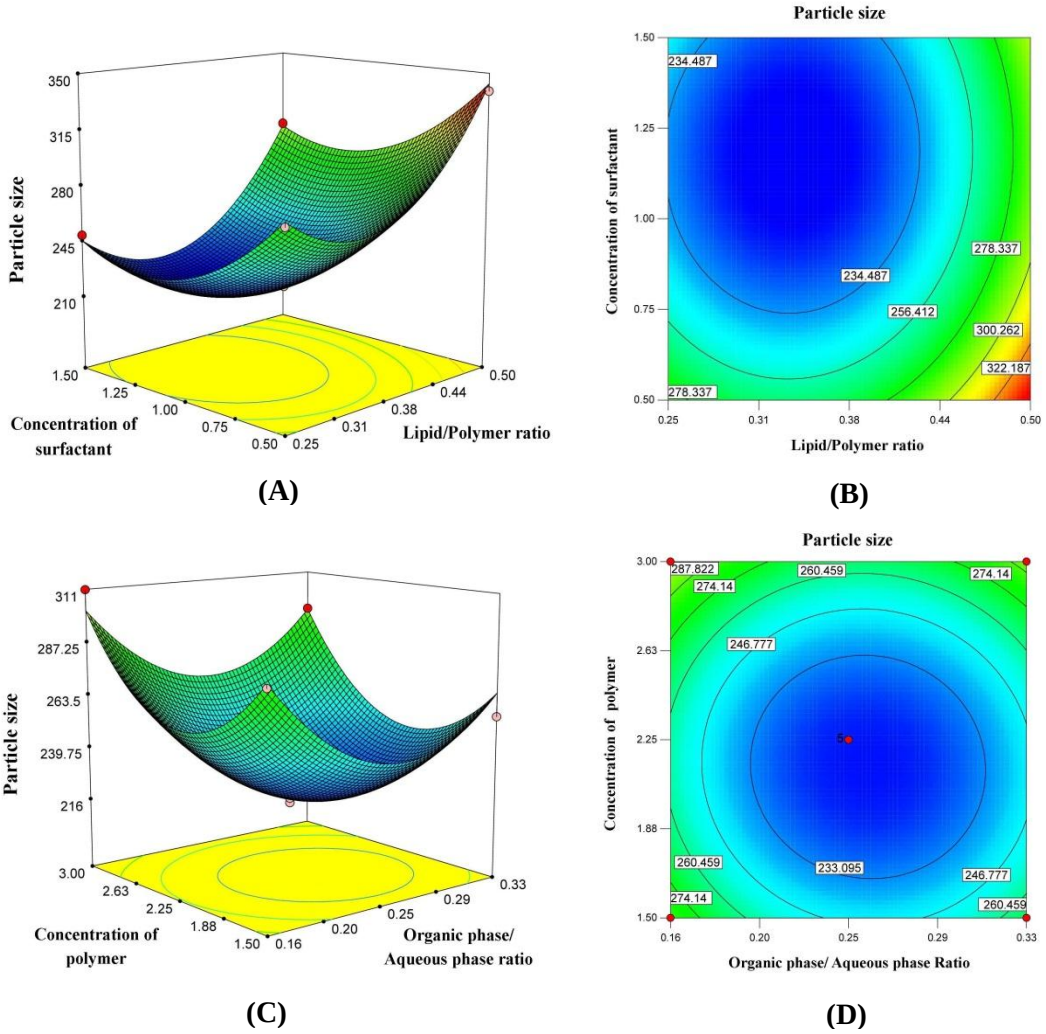

Figure 7.4 3D response surface plots (A), (C) and 2D contour plots (B), (D) showing the effect of independent variables (lipid/polymer ratio, concentration of surfactant, organic phase/aqueous phase ratio and concentration of polymer) on particle size of CS-PLHNs.

Similarly, organic phase/aqueous phase ratio (X_3) showed inverse relationship with particle size of CS-PLHNs. This could be attributed to the fact that large amount of organic solvent would decrease the viscosity as well as concentration of other components and thereby, impart high shear stress, which would result in breakdown

of emulsion droplets without any coalescence. It also favors the faster diffusion of organic phase into aqueous phase and ultimately results in nucleation of smaller-sized emulsion droplets, and thus smaller sized particles [54, 214].

The particle size increased significantly with increase in polymer concentration (X_4) might be because of triggering of the polymer-polymer interaction coupled with viscosity of the dispersed phase, which would result in formation of coarse dispersion with marked density difference. According to Stoke's law, the resultant density difference between aqueous and organic phase propels particle collisions by retarding the faster diffusion of organic solvent into external aqueous phase and thereby, favors aggregations which are difficult to be broken up using the same energy of mixing [182, 214, 245].

7.2.2.2.2 Influence of Independent variables on encapsulation efficiency

EE of developed CS-PLHNs was found to be varying in the range from 51.3 $\pm$ 2.4 % to 63.6 $\pm$ 1.6 % for different formulation variable combinations. The quadratic model was selected for the statistical analysis of influence of independent variables on EE of CS-PLHNs based on the lack of fit test as shown in Table 7.9. The second-order polynomial equation relating the EE (Y_2) and independent variables, generated by multiple linear regressions can be represented as follow in terms of coded variables:

$$Y_2 = 59.78 + 4.21X_1 - 2.80X_2 - 0.69X_3 + 1.43X_4 - 2.00X_2X_4 - 2.24X_2^2 - 1.40X_3^2 - 1.34X_4^2 \quad \text{Eq (7.2)}$$

Non-significant lack of fit value (p=0.3977; p>0.05) with F-value of 1.40 indicated that quadratic model is best fit to the independent variables for significantly describing the influence on the EE. Good correlation between experimental and predicted values was noticed as revealed by R^2 value of 0.9653. The minimal

difference between predicted R^2 (0.8323) and adjusted R^2 (0.9306) value indicated the adequacy of the selected model for the prediction of response. The value of adequate precision was found to be 19.227 (greater than 4 is desirable), suggesting an adequate signal to measure the signal independent of noise. Further, low value for coefficient of variation (1.76 %) indicated high degree of precision and reliability of the model. Thus, all the above consideration indicated that the present quadratic model for EE can be used to navigate the design space [23, 54, 179, 212].

Statistical analysis revealed that lipid/polymer ratio (X_1) and concentration of polymer (X_4) affects positively, whereas concentration of surfactant (X_2) and organic phase/aqueous phase ratio (X_3) provides negative effect on EE of CS-PLHNs. Also higher coefficient value (4.21) of lipid/polymer ratio (X_1) suggested that it had most significant effect on EE followed by concentration of surfactant (X_2), concentration of polymer (X_4) and organic phase/aqueous phase ratio (X_3). While in case of the interaction effects between different independent variables, only concentration of surfactant and concentration of polymer (X_2X_4) had combined significant effect on EE. However, effect of independent variables on EE is lower than the effect on particle size. This is because of the lower coefficient value of the main effects and interaction terms in the polynomial equation of EE compared with the polynomial equation of particle size [54, 179]. 3D response surface plots and 2D contour plots portraying the effect of independent variables on EE of CS-PLHNs are shown in Figure 7.5.

The lipid/polymer ratio (X_1) was found to increase EE of CS-PLHNs. Perhaps high lipid/polymer ratio provided thick lipidic barrier surrounding the polymeric core, which would have curtailed the diffusion of the drug towards the external aqueous phase [35]. Conversely, EE was found to decrease with an increase in surfactant

concentration (X_2). This could be explained by the fact that the higher surfactant concentration increases drug solubility by reducing interfacial tension and increasing partition of drug into aqueous phase, which in turn substantially lowers EE [208, 218].

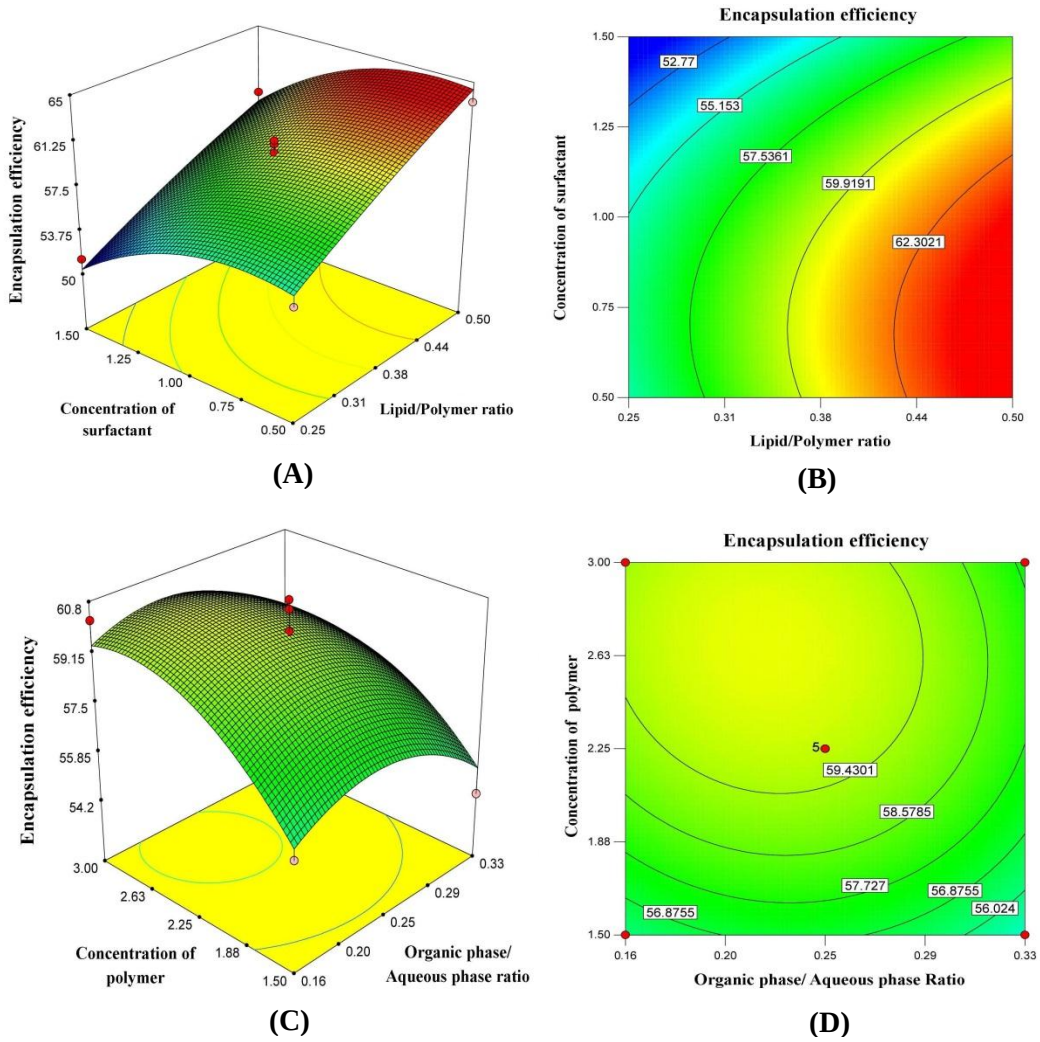

Figure 7.5 3D response surface plots (A), (C) and 2D contour plots (B), (D) showing the effect of independent variables (lipid/polymer ratio, concentration of surfactant, organic phase/aqueous phase ratio and concentration of polymer) on encapsulation efficiency of CS-PLHNs.

Likewise, the organic phase/aqueous phase ratio (X_3) was also negatively related to EE, probably as a result of enhanced partition of the drug into aqueous phase due to decreased viscosity of diffusion barrier. The reduction in viscosity facilitates rapid

diffusion of drug during emulsification and evaporation step owing to high shear stress, which ultimately results in CS-PLHNs with low drug payload [54, 218]. However, concentration of polymer (X_4) showed positive effect on EE of CS-PLHNs, which accordant with published literature that higher EE was obtained with higher polymer concentration due to rise in viscosity as well as faster solidification [208]. Additionally, increased polymer concentration would increase diffusion path length by forming larger sized CS-PLHNs and also form interfacial viscous diffusion barrier, which would further favor the encapsulation by restricting the drug diffusion towards the external aqueous phase [216].

7.2.2.2.3 Influence of independent variables on polydispersity index

The CS-PLHNs exhibited relatively narrow particle size distribution varied from minimum of 0.141 $\pm$ 0.099 to maximum of 0.389 $\pm$ 0.024, for selected level combination of different independent variables. Low PDI values nearer to 0 indicate the relative homogenous nature of the dispersion. The quadratic model was selected for the statistical analysis of influence of independent variables on PDI based on the lack of fit test as shown in Table 7.9. The quadratic model proposed the following second-order polynomial equation (Eq (7.3)) describing the relationship between independent variables and PDI (Y_3) in terms of coded variables.

$$Y_3 = 0.15 + 0.066X_1 - 0.049X_2 - 0.0082X_3 + 0.021X_4 + 0.017\ X_2X_3 - 0.037X_2X_4 + 0.085X_1^2 + 0.052X_2^2 + 0.061X_3^2 + 0.064X_4^2 \quad \text{Eq (7.3)}$$

The F-value of 5.62 with the absence of lack of fit value (p=0.0554; p>0.05) for quadratic model proves the excellent adequacy for significantly describing the influence of independent variables on the PDI. The higher R^2 value of 0.9861 suggests that 98.61% of variation in PDI was best explained by the formulation

variables. The adequacy of the selected regression model for the prediction of response was supported by the minimal difference between predicted R^2 (0.9239) and adjusted R^2 (0.9722) value. The value of adequate precision was found to be 26.579 (greater than 4 is desirable), suggesting an adequate signal to measure the signal independent of noise. Further, low value for coefficient of variation (5.13 %) indicated high degree of precision and reliability of the model. Therefore, the proposed quadratic model can be employed in order to navigate the design space [23, 54, 179, 212].

Statistical analysis revealed that lipid/polymer ratio (X_1) and concentration of polymer (X_4) affects positively, whereas concentration of surfactant (X_2) and organic phase/aqueous phase ratio (X_3) provides negative effect on PDI of CS-PLHNs. Also higher coefficient value (0.066) of lipid/polymer ratio (X_1) suggested that it had most significant effect on PDI followed by concentration of surfactant (X_2), concentration of polymer (X_4) and organic phase/aqueous phase ratio (X_3). While in case of the interaction effects between different independent variables, concentration of surfactant and organic phase/aqueous phase ratio (X_2X_3) as well as concentration of surfactant and concentration of polymer (X_2X_4) had combined significant effect on PDI. However, effect of independent variables on PDI is lowest than the effect on particle size and EE. This is because of the lower coefficient value of the main effects and interaction terms in the polynomial equation of PDI compared with the polynomial equation of particle size and EE [54, 179]. 3D response surface plots and 2D contour plots portraying the effect of independent variables on PDI of CS-PLHNs are depicted in Figure 7.6.

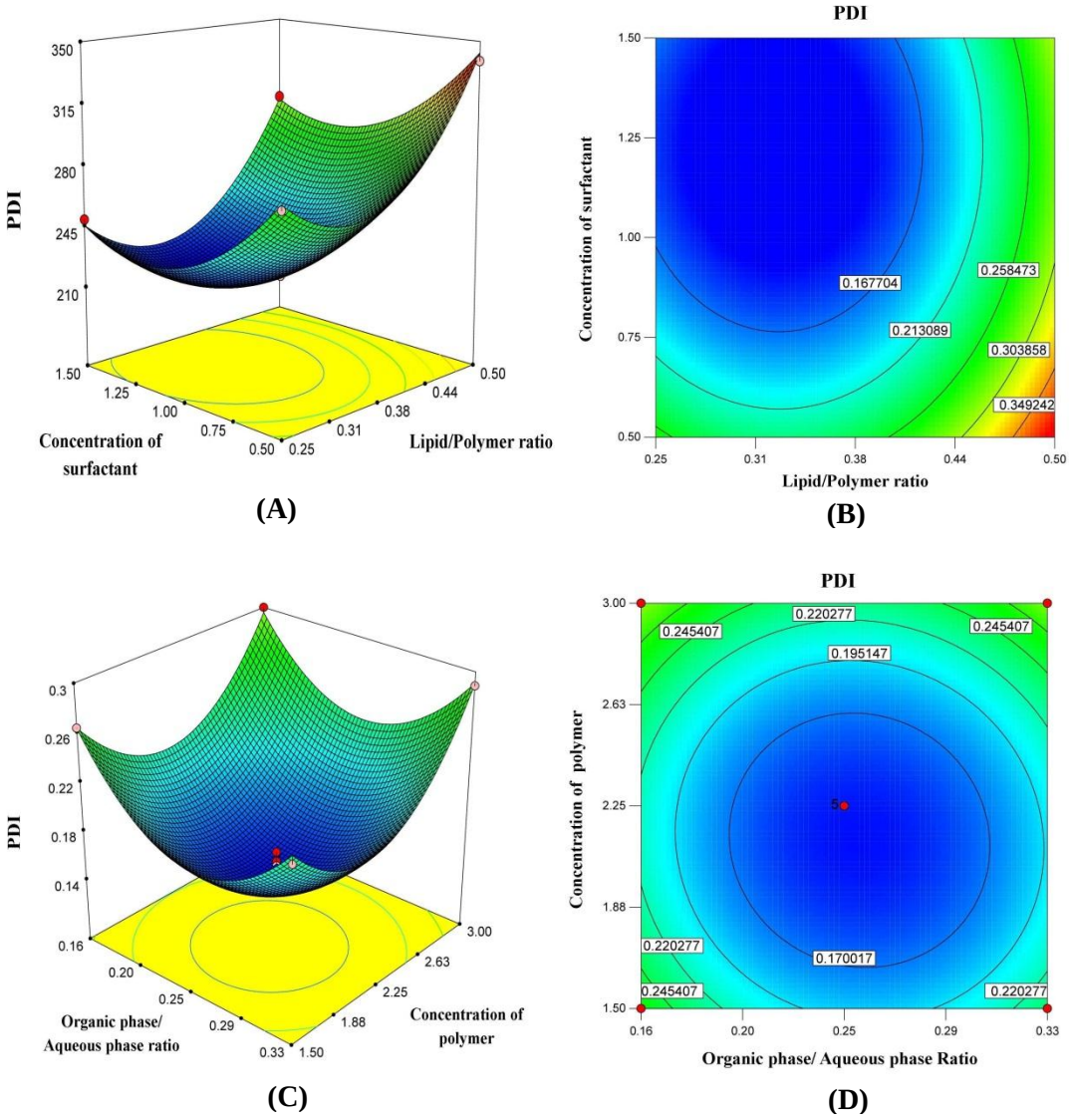

Figure 7.6 3D response surface plots (A), (C) and 2D contour plots (B), (D) showing the effect of independent variables (lipid/polymer ratio, concentration of surfactant, organic phase/aqueous phase ratio and concentration of polymer) on PDI of CS-PLHNs.

The lipid/polymer ratio (X_1) exhibited significant positive influence on PDI owing to its direct impact on the thickness of the lipid covering over the polymeric core. Higher lipid/polymer ratio would have accelerated the aggregation by suppresing their native surface charge, which would result uneven size distribution. Moreover, formation of single and multilamellar liposomes at higher lipid concentration also enforces the

polydispersity [23, 54]. Nevertheless, significant drop in polydispersity was noticed at elevated surfactant concentration (X_2) and organic phase/aqueous phase ratio (X_3), could be attributed to the marked reduction in the interfacial tension as well as dilution of polymer and lipid concentration, as reported earlier. The reduction in interfacial tension between aqueous phase and organic phase ensures good emulsification process, imparting homogeneity to CS-PLHNs [205]. The polymer concentration (X_4) exhibited positive relationship with PDI on account of its direct impact on emulsification efficiency. Higher polymer concentration could favor the formation of coarse dispersion due to lack of sufficient energy to overcome the resistive viscous forces as well as lack of sufficient surfactant concentration for stabilization of newly generated particles, which could have ultimately imposed the polydispersity to CS-LPHNs [214, 219].

7.2.2.2.4 Optimization of CS-PLHNs using desirability function

Optimization of formulation by considering all the objectives at a time is difficult because of opposite effect of various independent variables. The optimum level of one independent variable might result in an inverse effect for other independent variable. Hence, a numerical optimization technique using desirability function was probed for simultaneous optimization of the four independent variables, which would yield CS-PLHNs with desired quality traits. The levels of four different independent variables were determined using Design-Expert® software by fixing different constraints, which would yield maximum EE with minimum particle size and PDI. The optimized CS-PLHNs were formulated using predicted levels of respective independent variables for confirming the validity as well as predictive capability of experimental design as shown in Table 7.10. The desirability of the optimized CS-PLHNs was 0.866. The close proximity with low percentage of bias between predicted results and

experimental results reaffirmed the reliability of prognostic ability of Box Behnken experimental design for statistical optimization of desirable CS-PLHNs [23, 179, 182, 183].

Table 7.10 Comparison of experimental and predicted values of optimized CS-PLHNs with its desirability generated by Design expert®

Independent variables	**Optimized levels**		
Lipid/polymer ratio (X_1)	0.37		
Concentration of surfactant (X_2)	1.01 % w/v		
Organic phase/aqueous phase ratio (X_3)	0.25		
Concentration of polymer (X_4)	2.25 % w/v		
Results			
	Experimental values	**Predicted values**	**% Bias***
Particle size (nm)	227 ± 3.8	219.95	-3.20
Encapsulation efficiency (%)	57.8 ± 1.32	59.69	3.16
Polydispersity index (PDI)	0.151 ± 0.027	0.145	-4.13
Overall Desirability	0.866		
Drug loading (%)	4.28 ± 0.23		
Zeta potential (mV)	(-) 27.8 ± 1.8		

**Bias was calculated as [(predicted value-experimental value)/predicted value] X 100;*
All results are shown as mean ±S.D; n=3.

Optimized CS-PLHNs were further selected for various *in-vitro* and *in-vivo* characterization studies. The useful results obtained by statistical analysis of data reiterated the utility of "Quality by Design" approach in performing experiments.

7.2.3 Characterizations of CS-PLHNs

7.2.3.1 Solid state characterizations

7.2.3.1.1 Fourier transform infrared spectroscopy (FTIR) study

FTIR study was performed in order to evaluate chemical stability and to identify the significant change, if occurs during the encapsulation of CS inside the PLHNs. The FTIR spectra for pure CS, PLGA, soya lecithin, PVA and optimized CS-PLHNs are shown in Figure 7.7. As depicted in Figure 7.7 (a), FTIR spectra of CS exhibited two basic characteristic peaks at 1640 cm^{-1} and 3416 cm^{-1} indicative of C=O stretching and O-H stretching, respectively. The characteristic peaks at 2880 cm^{-1} 1477 cm^{-1}, 1573 cm^{-1} and 1410 cm^{-1} are assigned to the alkane C-H, aromatic C-H, asymmetric and symmetric COO^{-}, respectively. Additionally, large number of characteristic absorption bands in fingerprint region (1400-600 cm^{-1}), were noticed as a result of vibration within the molecule [43, 45]. The FTIR spectra of PLGA (Figure 7.7 (b)) showed that the significant peaks of PLGA are C=O stretching at 1748 cm^{-1}, C-O stretching at 1194 cm^{-1}, C-H stretching at 2948 cm^{-1} and broad bands between 3200-3600 cm^{-1} due to its terminal hydroxyl group [205]. The FTIR spectra of soya lecithin (Figure 7.7 (c)) showed characteristic band in the range of 1765-1720 cm^{-1} corresponding to the C=O vibration and another band in the range of 1200-1145 cm^{-1} due to the PO_2 vibration. Additionally, some bands in the range of 1200-970 cm^{-1} were noticed corresponding to both P-O-C as well as PO_2 vibrations, respectively [244]. In case of FTIR spectra of PVA (Figure 7.7 (d)), major peaks in the range of 2840-3000 cm^{-1} for C-H stretching, 3200-3550 cm^{-1} for O-H stretching, 1290 cm^{-1} for C-N stretching and 1750-1735 cm^{-1} for C=O as well as C-O stretching from acetate group were observed [206]. All the major peaks pertaining to CS were retained in the

FTIR spectra of optimized CS-PLHNs (Figure 7.7 (e)) with little variations in their frequencies, confirming the successful encapsulation of CS inside the matrix of PLHNs without any change in its chemical nature during the encapsulation process [23, 49, 221].

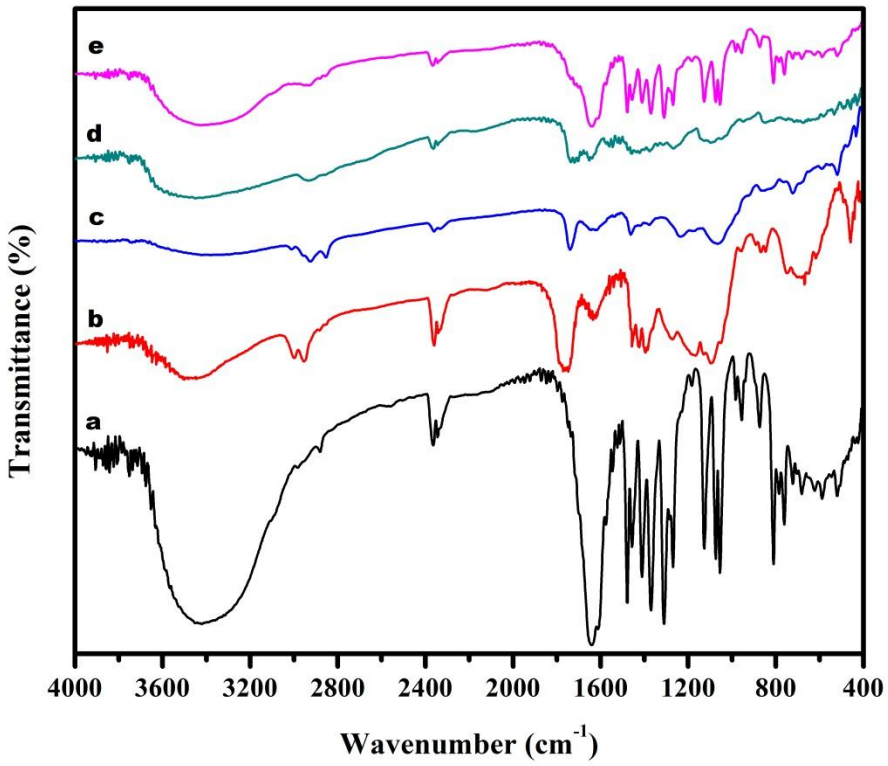

Figure 7.7 FTIR spectra of (a) CS, (b) PLGA, (c) soya lecithin, (d) PVA and (e) optimized CS-PLHNs

7.2.3.1.2 Differential scanning calorimetry (DSC) study

DSC thermograms of CS, PLGA, soya lecithin, PVA and optimized CS-PLHNs are depicted in Figure 7.8. In the DSC thermogram of pure CS, sharp melting endotherm appeared at 264 ^{o}C attributed to its melting point, indicating its crystalline behaviour. Further, any peaks due to release of absorbed moisture or nonstructural water as well

as solid state transitions were not identified [49, 149, 210]. PLGA exhibited sharp endothermic peak at 65 ^{o}C.

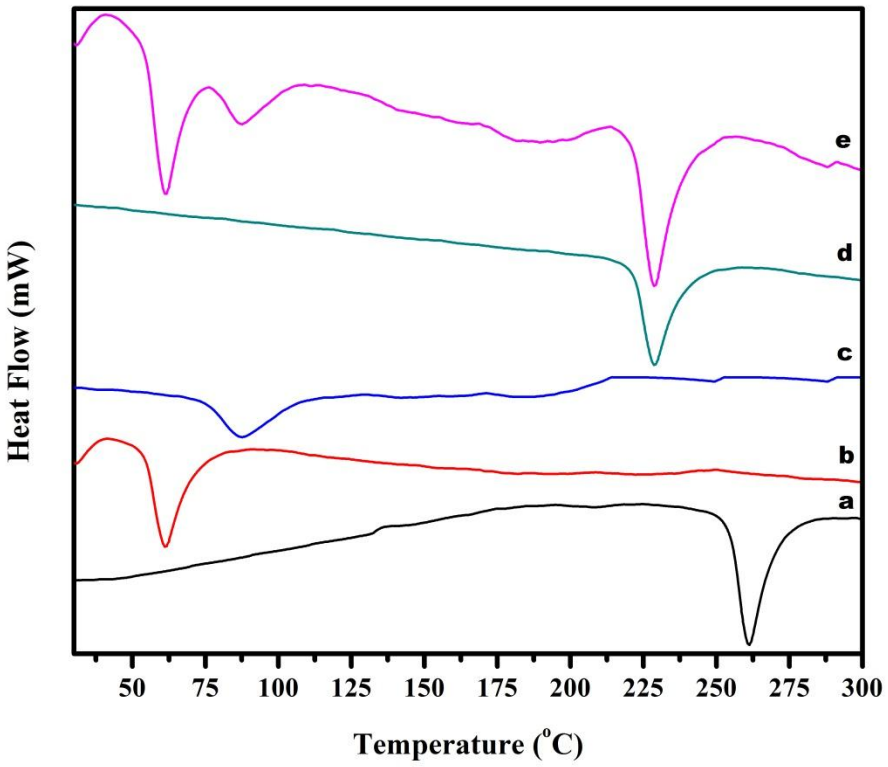

Figure 7.8 DSC thermograms of (a) CS, (b) PLGA, (c) soya lecithin, (d) PVA and (e) optimized CS-PLHNs.

Soya lecithin displayed broad endothermic peak at 87 ^{o}C corresponding to its phase transition. PVA showed sharp endotherm at 226 ^{o}C corresponding to its melting point. Contrary, the absence of characteristic melting endotherm of CS in the thermogram of CS-PLHNs (Figure 7.8 (e)) suggested that the phase transformation of CS from crystalline state to amorphous state has taken place during the encapsulation process and CS is dispersed as an amorphous molecular dispersion for inside the matrix of CS-PLHNs. The shear stress provided by the stirrer during the fabrication process of PLHNs might have prevented the recrystallization of CS from its tiny

droplets, leaving CS in an amorphous molecular dispersion form inside the PLHNs [188, 247]. The thermal behaviour of other excipients remained same as their pure thermograms. Furthermore, the absence of any new redundant endothermic peaks in the thermogram of CS-PLHNs confirmed the homogeneous encapsulation of CS inside the matrix of PLHNs without any interactions [207, 210, 224].

7.2.3.1.3 Powder X-ray diffractometry (PXRD) study

Powder X-ray diffractogarms of pure CS, PLGA, soya lecithin, PVA, their physical mixture and optimized CS-PLHNs are depicted in Figure 7.9. The powder X-ray diffraction pattern of pure CS displayed characteristic distinctive peaks at 2θ angles of 8º, 9.83º, 11.5º, 14º, 16.9º, 19.7º, 24.3º, 26.6º and numerous minor peaks up to 35º as illustrated in Figure 7.9 (a). The intense, sharp and well resolved peaks indicated that CS is highly crystalline in nature [45, 149]. The diffraction patterns of the PLGA, PVA and soya lecithin exhibited number of small diffuse peaks with broad halo [23, 205]. The diffractogram of physical mixture (Figure 7.9 (e)) showed all the sharp crystalline peaks of the CS, nearly at the same scattering 2θ angles as appeared in pure form, indicating the retention of its crystalline behaviour without any physical change. Since PLGA, soya lecithin and PVA exhibited no any characteristic diffraction peaks, the crystalline peaks must be originated from the crystalline region of CS due to absence of any interaction. Oppositely, the PXRD pattern of CS-PLHNs (Figure 7.9 (f)) exhibited that all the characteristic sharp peaks of CS were abridged in their intensity and converted into broad, diffuse peaks. The stifling of diffraction intensity of CS confirmed that the physical state of CS was transformed towards an amorphous molecular dispersion form upon encapsulation inside the PLHNs [210, 226]. PXRD results are in good agreement with the results demonstrated by DSC,

confirming the homogeneous and complete encapsulation of CS inside the hybrid matrix of the LPHNs [23, 224, 248].

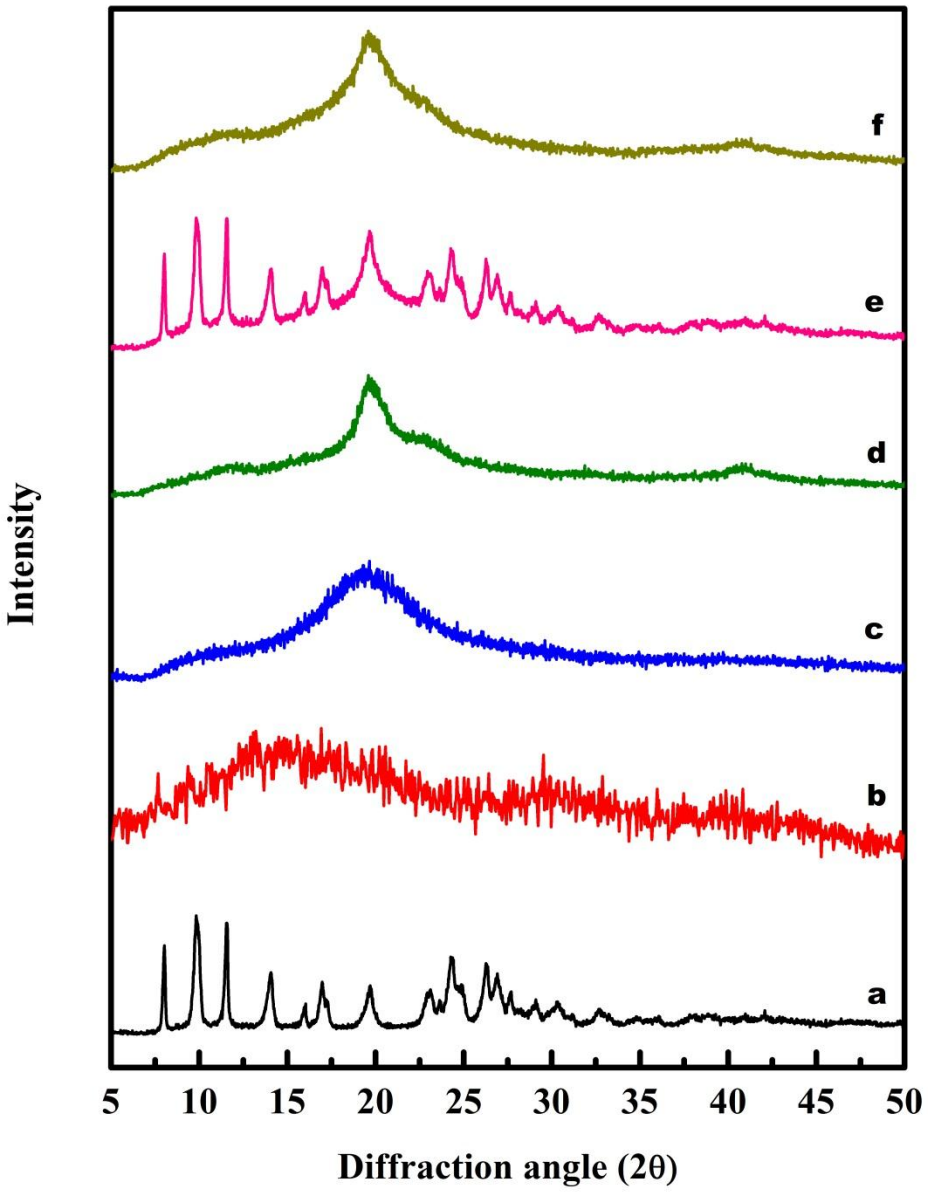

Figure 7.9 PXRD patterns of (a) CS, (b) PLGA, (c) soya lecithin, (d) PVA, (e) physical mixture and (f) optimized CS-PLHNs.

7.2.3.2 Shape and surface morphology

7.2.3.2.1 High resolution transmission electron microscopy (HR-TEM)

The shape and surface morphology of the optimized CS-PLHNs was examined by employing HR-TEM. The HR-TEM micrographs (Figure 7.10 (A)) revealed that the developed CS-PLHNs were discrete, homogeneous and spherical in shape having uniform size distribution. High magnification indicated that CS-PLHNs were appeared as spherical particles which have an inner dark polymeric core surrounded by the lighter phospholipid envelop. The core-shell structure of CS-PLHNs was clearly visible due to the marked electron density difference between polymer and lipid [50]. The external surface of CS-PLHNs was observed as smooth without any visible, rough pores or ruptures. The particle size obtained with HR-TEM micrographs was comparable to that obtained by particle size analyzer using dynamic light scattering technique, in which most of them are smaller than 250 nm.

Additionally, the electron diffraction (ED) pattern of CS-PLHNs was generated by HR-TEM in order to confirm the physical state of CS inside the matrix of PLHNs. The ED pattern (Figure 7.10 (B)) exhibited smooth diffraction halo pattern with absence of star shaped, bright spots in its circular diffraction ring pattern, which confirmed the encapsulation of CS as homogeneous, amorphous dispersion form inside the matrix of PLHNs [23, 198, 226], further substantiating the inference deduced from DSC and XRD results.

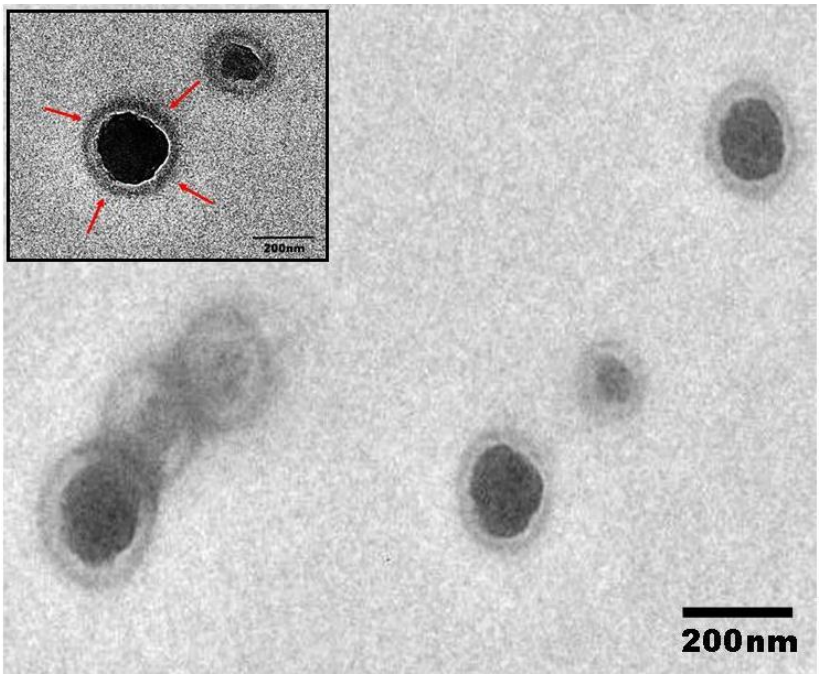

(A)

(B)

Figure 7.10 (A) HR-TEM image of optimized CS-PLHNs, Inset image shows core-shell architecture of the CS-PLHNs; (B) Electron diffraction pattern of optimized CS-PLHNs

7.2.3.2.2 Atomic force microscopy (AFM)

The surface morphology of optimized CS-PLHNs was further determined by AFM study in order to confirm the morphological aspect revealed by HR-TEM. The topographic and 3D AFM micrographs of CS-PLHNs, generated by the atomic level interaction between a sharp probing tip and the surface of CS-PLHNs are depicted in Figure 7.11 (A) & (B).

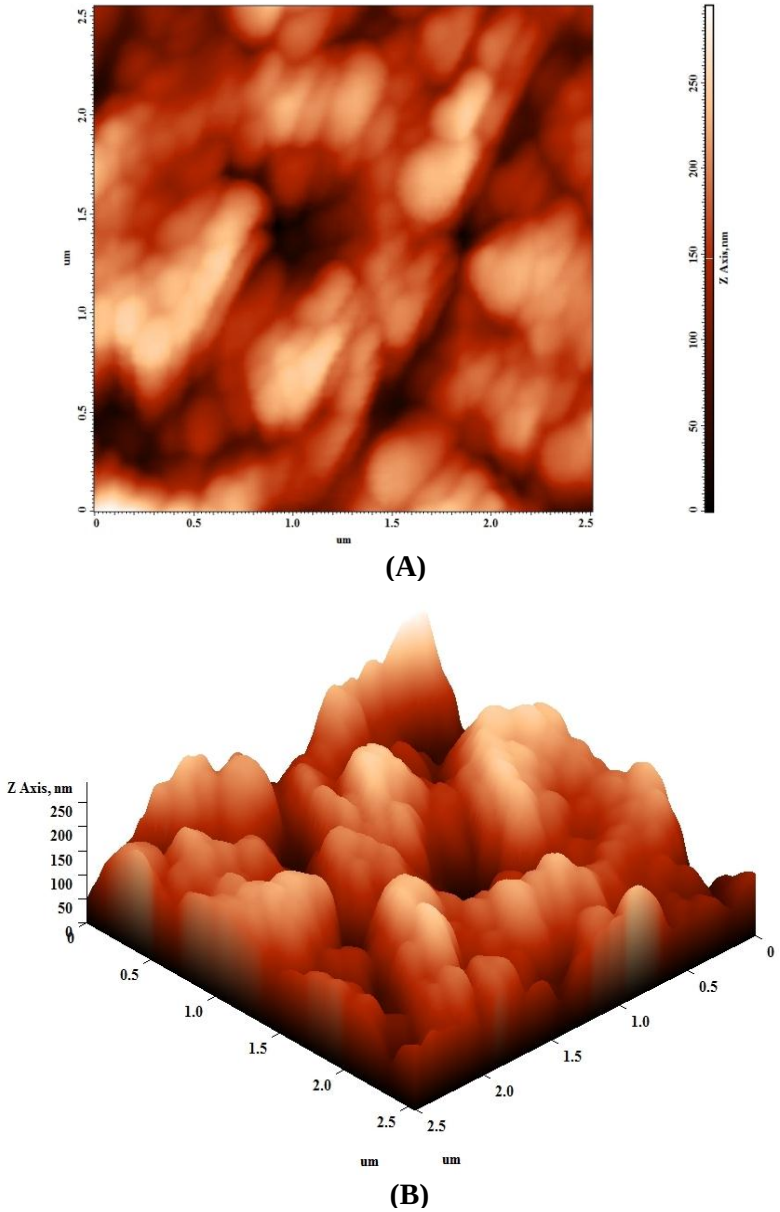

(A)

(B)

Figure 7.11 AFM images of optimized CS-PLHNs (A) 2D micrograph and (B) corresponding 3D micrographs.

The particle size and surface morphology revealed by AFM was in accordance with the results of HR-TEM study. AFM images generated by direct analysis of originally hydrated CS-PLHNs sample, showed uniform spherical shaped CS-PLHNs having smooth surface without any visible crevices or pores. AFM micrographs displayed the well separated CS-PLHNs in the nanometric size range of below 250 nm with low polydispersity. The probable reason for smooth surface could be the uniform covering of lipid over the outer surface of polymeric core, which has resealed the pores or crevices generated by the diffusion of organic solvent during the encapsulation process [23, 188].

7.2.3.2.3 Confocal laser scanning microscopy (CLSM)

Further, core-shell type of architecture of CS-PLHNs was confirmed by CLSM study. The CLSM micrograph of fluorescent CS-PLHNs, generated by visualizing under confocal microscope showed clear differentiation of two regions of different material (Figure 7.12 (A) & (B)).

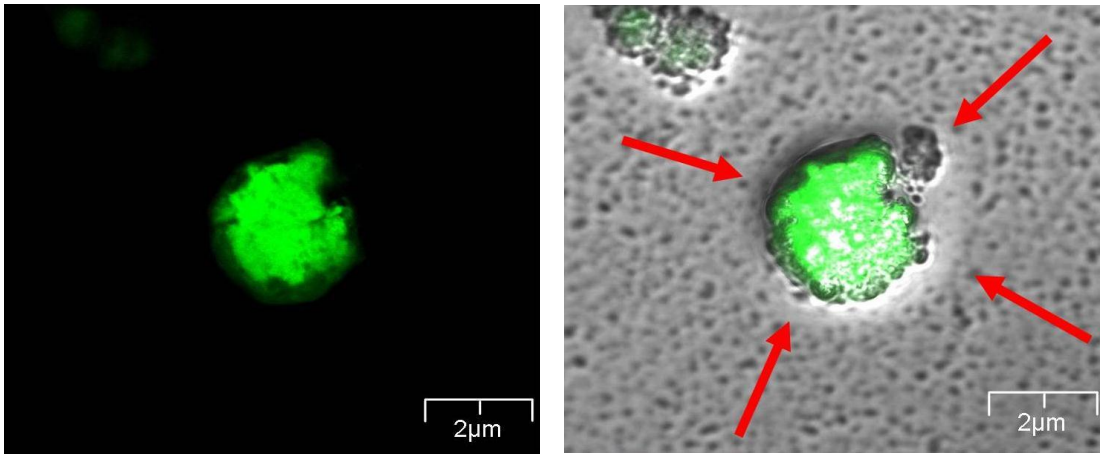

(A) **(B)**

Figure 7.12 (A) Fluorescent confocal microscopic image and (B) 3D - Confocal microscopic image of micron sized CS-PLHNs tagged with FITC, showing core-shell architecture

The green color represented the polymeric core, whereas very light circle surrounding the green color represented the colorless lipid envelop, which corroborates well with the findings of HR-TEM study [23].

7.2.3.3 *In-vitro* drug release study

In-vitro drug release study was performed in order to assess the potential of CS-PLHNs to control the release of CS for prolonging the action. *In-vitro* drug release profile of CS from CS-PLHNs showed the biphasic release pattern in phosphate buffer pH 7.4 as illustrated in Figure 7.13.

Table 7.11 *In-vitro* drug release data of the optimized CS-PLHNs in phosphate buffer pH 7.4

Time (hr)	Cumulative % drug release
0	0
1	16.99 ± 0.31
2	20.06 ± 0.32
3	22.19 ± 0.33
4	25.93 ± 0.52
5	29.67 ± 1.25
6	31.52 ± 0.55
7	34.30 ± 0.73
8	36.43 ± 1.28
10	40.04 ± 1.05
12	45.69 ± 2.00
18	61.71 ± 2.12
24	73.84 ± 1.69
36	91.89 ± 0.97
48	92.91 ± 1.21

All values reported are mean ± SD, (n=3)

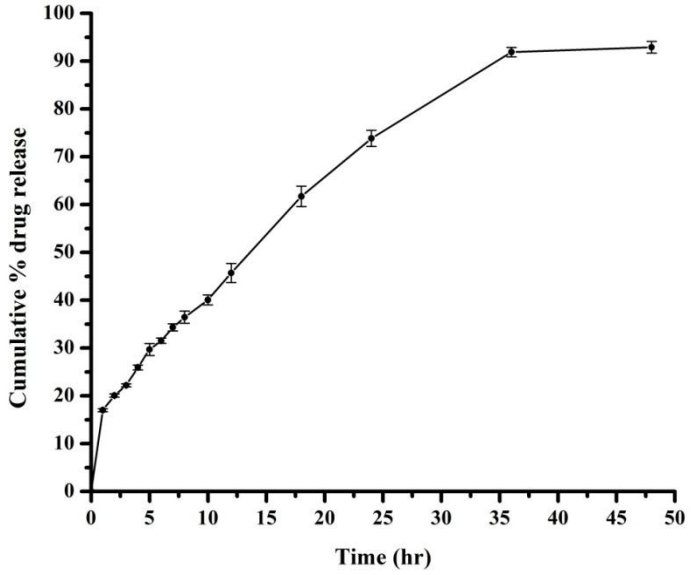

Figure 7.13 *In-vitro* drug release profile of optimized CS-PLHNs in phosphate buffer pH 7.4 (vertical bar represents ±S.D; n=3)

The CS release from CS-PLHNs showed phasic release behaviour, comprising of initial burst release followed by extended release over a period of 48 hr. The optimized CS-PLHNs exhibited around 93% drug release at the end of 48 hr. The superclass II release was noticed up to 1 hr with an initial burst of nearly 17 % of the drug. This might likely be due to the rapid diffusion and desorption of surface adsorbed or weakly bounded drug as well as partial erosion of the outer phospholipid layer of CS-PLHNs, which resulted in quicker diffusion of hydrophilic drug as reported earlier [248]. The subsequent extended release was achieved up to 48 hr, indicating the slower diffusion of the encapsulated CS from CS-PLHNs (Table 7.11). The sustained release might be ascribed to the lipidic barrier provided by phospholipid envelop, which has restricted the penetration of release medium and curtailed the faster immobilization of the CS from the polymeric core and thereby, extended the release [36]. Additionally, hydration and swelling of polymer causes

substantial increment in the diffusional path length, which eventually slowdowns the diffusion of drug molecules form the nanoparticles [227].

Furthermore, the drug release mechanism and kinetics were determined by substituting the drug release profile data of CS-PLHNs to different release kinetic models (i.e., zero order, first order, Higuchi model and Korsmeyer-Peppas model). The release kinetic modeling suggested that the drug release pattern of CS from the CS-PLHNs was best explained by Higuchi model, indicating matrix diffusion controlled release process (highest R^2 value compared to other kinetic models as shown in Table 7.12). Further, the release exponent (n) value obtained by fitting Korsmeyer-Peppas semi empirical model was found to be 0.493, which is suggestive that the drug release occurred through fickian diffusion based controlled release pattern from the matrix of the CS-PLHNs ($n<0.5$ for fickian diffusion) [191, 192]. This is expected since the CS being hydrophilic drug molecule; it has a greater tendency for diffusion, as per the previously reported scientific literature for the hydrophilic drug [243]. Hence, it is possible to achieve fluctuation free steady state CS plasma level upon oral administration of CS-PLHNs, which provides loading dose due to initial burst release followed by maintenance dose for extended period of time [23, 49].

Table 7.12 Release kinetic models for simulation of release behaviour of CS from optimized CS-PLHNs in phosphate buffer pH 7.4

Batch	Zero Order	First Order	Higuchi Model	Korsemeyer-Peppas model
Optimized CS-PLHNs	$R^2 = 0.9416$ $K_z = 1.781$	$R^2 = 0.8341$ $K_F = 0.0356$	$R^2 = 0.9804$ $K_H = 14.573$	$R^2 = 0.9745$ $K_P = 13.934$ $n = 0.4934$

7.2.3.4 Accelerated and real time storage stability study

The ability of any colloidal system to remain stable against environmental changes is of prime requirement to ensure its final performance in terms of its *in-vivo* fate. Nanoparticles have very high tendency to agglomerate owing to their large surface-area-to-volume ratio, which results in the increase in particle size after longer periods of storage. Changes in the physical appearance, color, odor, taste, or texture of the formulation indicate the instability. The stability and intactness of CS-PLHNs was assessed over a period of 6 month at room temperature (25 $\pm$ 2 ^{o}C), refrigerated condition (4 $\pm$ 1 ^{o}C), and accelerated condition (40 $\pm$ 2 ^{o}C/75 $\pm$ 5 % RH). The physical appearance and physicochemical attributes (i.e., particle size, EE and PDI) were chosen as stability indicating parameters. The changes in the physicochemical attributes of the CS-PLHNs during the stability study over the period of 6 months are depicted in Figure 7.14.

The physical appearance of the CS-PLHNs did not show any significant difference (i.e., lump formation and discoloration) at different environmental conditions during the study. Depositions formed on the base of container during storage were easily redispersible on mere shaking. Additionally, insignificant change (p>0.05) in the particle size, PDI and EE was noticed for CS-PLHNs, stored at room temperature (25 $\pm$ 2 ^{o}C) and refrigerated condition (4 $\pm$ 1 ^{o}C) over a period of 6 month.

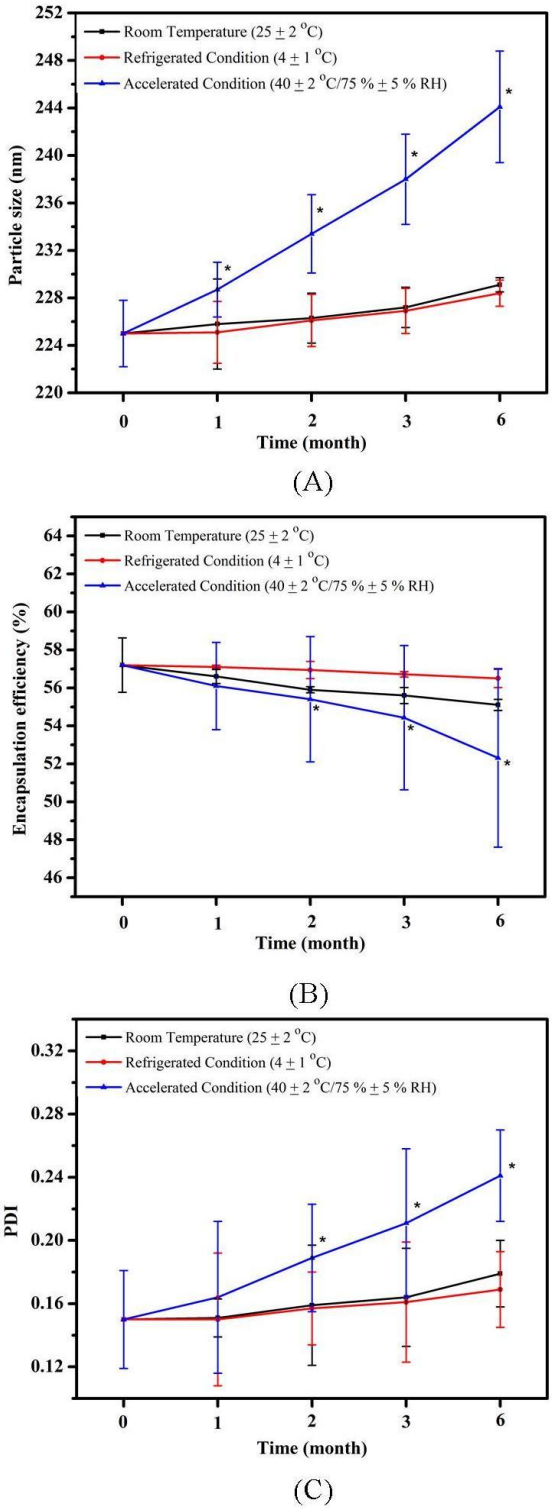

Figure 7.14 Effect on (A) particle size, (B) encapsulation efficiency and (c) PDI of optimized CS-PLHNs stored at different environmental conditions over different time interval (vertical bars represent ± SD; n=3); *significant at $p<0.05$ compared with 0 time

However, significant difference (p<0.05) in the particle size, PDI and EE was observed for the CS-PLHNs stored at accelerated condition (40 ± 2 °C/75 ± 5 % RH), indicating the instability of the formulation at that environmental condition. The instability might be due to conglomeration of the CS-PLHNs offered by hygroscopic soya lecithin molecules and degradation of the polymer, which would have expelled the drug molecule from hybrid nanostructures [23]. Hence, it is strongly recommended that developed CS-PLHNs should be stored at below room temperature (<25 °C) or at refrigerated condition (4 ± 1 °C), in order to retain their pharmaceutical properties for safe and effective long-term usage [49, 193, 228, 229].

7.2.3.5 *Ex-vivo* intestinal permeation study

The *ex-vivo* permeation study using non-everted rat intestinal model was accomplished in order to assess the intestinal permeation potential of CS-PLHNs. The significant improvement in the intestinal permeation of CS, approximately ~6 folds (p<0.05) was observed by encapsulating inside PLHNs compared to CS solution (Table 7.13). Figure 7.15 represents the intestinal permeation profile of CS from CS solution and CS-PLHNs, along with their apparent permeability coefficient (Papp). The Papp value for CS from CS solution and CS-PLHNs were found to be 0.909 (± 0.049) × 10^{-5} cm/s and 5.441 (± 0.373) × 10^{-5} cm/s, respectively. The high hydrophilicity offered by the tween carboxylic group of the CS might be responsible for poor permeation of CS across rat intestine [43, 45]. The permeability enhancement ratio for CS was found to be 5.98 ± 0.74 by developing CS-PLHNs (Figure 7.16).

Table 7.13 *Ex-vivo* permeation data of the CS solution and optimized CS-PLHNs across rat intestinal membrane

Time (min)	Cumulative % drug permeated	
	CS solution	CS-PLHNs
0	0	0
15	1.21 ± 0.039	4.28 ± 0.08
30	2.40 ± 0.021	9.34 ± 1.02
45	3.33 ± 0.053	12.08 ± 1.08
60	4.39 ± 0.052	20.09 ± 2.23
90	4.98 ± 0.083	29.15 ± 1.83
120	5.71 ± 0.539	36.47 ± 1.94
180	6.78 ± 0.504	44.89 ± 2.81
240	7.71 ± 0.588	54.40 ± 2.72

All values reported are mean ± SD, (n=3)

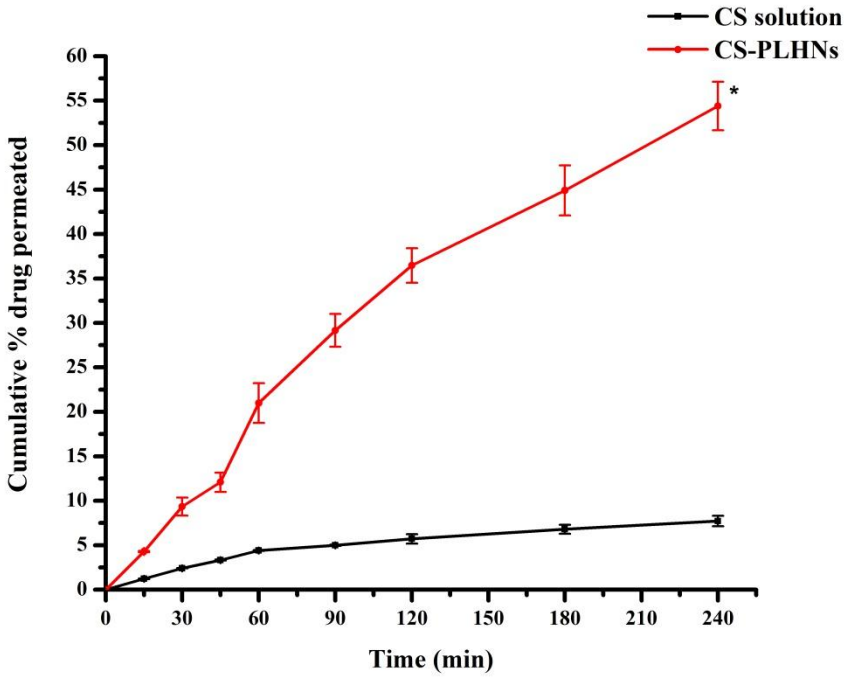

Figure 7.15 *Ex-vivo* permeation study of CS-PLHNs and CS solution across rat intestinal membrane. Vertical bars represent ± SD; n=3, *significant at $p<0.05$ compared with CS solution (Unpaired student t-test)

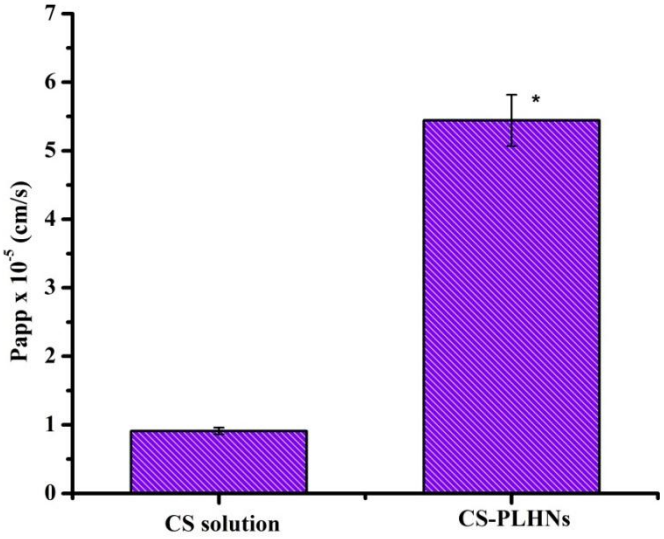

Figure 7.16 Apparent permeability coefficients (Papp) for CS from CS-PLHNs and CS solution. Vertical bars represent ± SD; n=3, *significant at p<0.05 compared with CS solution (Unpaired student t-test)

The observed significant high (p<0.05) permeation of CS in the form of CS-PLHNs at each time point compared to CS solution might be attributed to their nano-size as well as hydrophobic nature of lipid, which would have facilitated the absorption across intestine through specialized transport mechanisms [106, 107]. It has been previously reported that the nanoparticles of less than 500 nm are effectively absorbed via endocytosis through lymphoid tissues in the intestine [24]. Additionally, the enhanced interaction of CS-PLHNs with lipophilic biological membrane due to phospholipid envelop, might be also plausible reason for an effective endocytosis through enterocytes as well as selective uptake by M cells of PP, which eventually reflected via higher CS concentration in basolateral side [23, 35, 232, 249]. Results are in well corroboration with the hypothesis.

7.2.3.6 *In-vivo* intestinal uptake study

The *in-vivo* intestinal permeation potential of the CS-PLHNs was visualized using confocal microscopy after oral administration in the rats. FITC tagged CS-PLHNs were administered orally to the overnight fasted rats. The confocal microscopic images of the cross sections of rat intestinal tissue, showing the absorption of FITC tagged CS-PLHNs are portrayed in Figure 7.17.

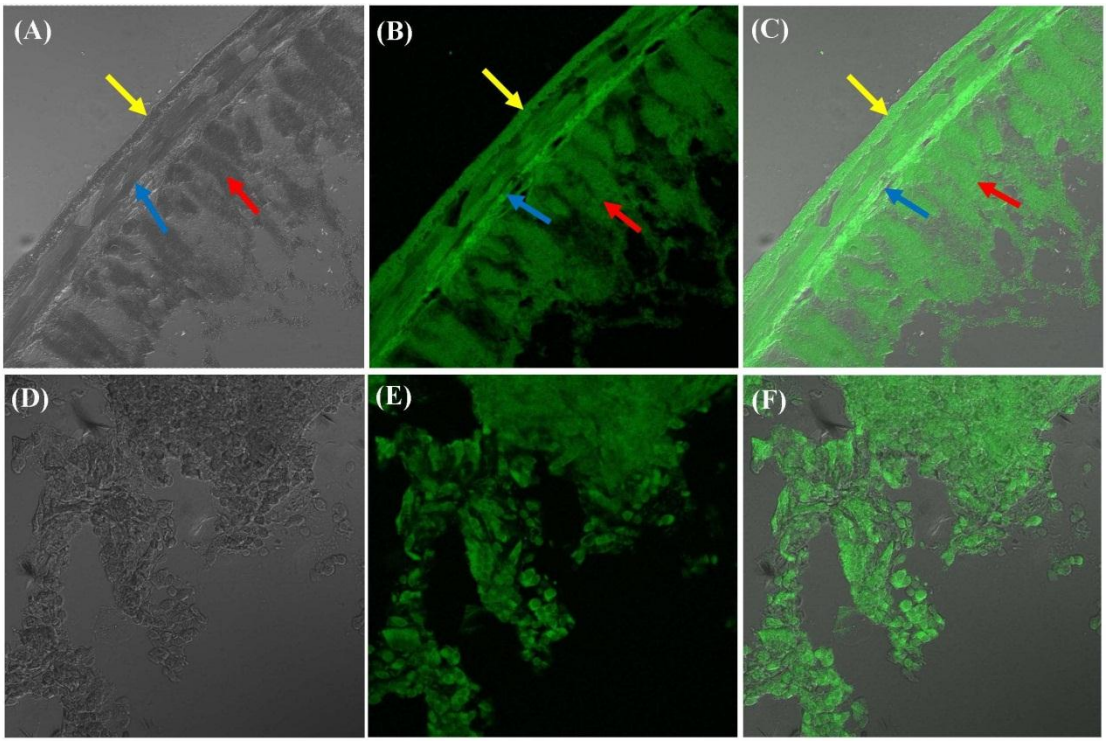

Figure 7.17 Confocal laser scanning micrographs of rat intestine, showing uptake and transport of FITC tagged CS-PLHNs into the tissues, underlying the absorptive cells, after 2 hr of oral administration. (A) DIC image; (B) Fluorescent image; and (C) Merge of fluorescent and DIC image scanned at 10× plain. (D) DIC image; (E) Fluorescent image; and (F) Merge of fluorescent and DIC image scanned at 40× plain using emersion oil objective. Red, blue and yellow arrows indicate the mucosal, submucosal, and muscular regions of rat intestine, respectively in transverse section

The strong green fluorescence attributed to FITC was noticed throughout the apical portion of the villi in the intestinal lumen, specifically mucosa and submucosa (blood and lymphatic vessels). The various stage of internalization and distribution of CS-PLHNs in the enterocytes and intestinal mucosa after 2 hr of administration suggested that, an effective endocytosis was taken place in the intestinal mucosal epithelia, PP of the follicle-associated epithelium and the underneath regions of the secondary lymphoid organ. The results confirmed that the CS-PLHNs were able to interact with intestinal barrier and be internalized by following various transportation mechanisms such as paracellular pathway, transcellular pathway through enterocytes and endocytosis by M-cells of PP [23, 49, 106, 196].

Additionally, a strong fluorescence was also observed at the surface of the villi conceivably as a consequence of CS-PLHNs' bioadhesion with the mucous layer of GIT wall. The mucoadhesivity imparted by the phospholipid envelop and surfactant layer (i.e., PVA) of CS-PLHNs, prolonged the residence time and thereby, improved the intestinal permeation by facilitating particulate interaction [24]. As CS remains encapsulated within the CS-PLHNs during the internalization process across GIT, it resulted in enhanced permeation, which further strengthens our hypothesis and the finding of *ex-vivo* studies. Hence, it can be concluded that LPHNs play an important role in the facilitating the CS permeation to systemic circulation through the intestinal membrane [233, 234, 250].

7.2.3.7 *In-vivo* pharmacokinetic study

The plasma drug concentration-time profiles obtained after the single dose oral administrations of the CS solution and CS-PLHNs in rats (20 mg/kg) are presented in Figure 7.18 and corresponding data are presented in Table 7. 14.

Table 7.14 Plasma drug concentration time profile data of CS solution and CS-PLHNs following single dose oral administration in rats

Time (hr)	Plasma concentration of CS (ng/ml)	
	CS solution	CS-PLHNs
0	0	0
0.25	11.42 ± 1.36	7.70 ± 1.04
0.5	50.59 ± 4.30	24.11 ± 2.08
1	112.23 ± 5.90	59.55 ± 2.35
2	70.08 ± 2.86	109.38 ± 6.83
4	28.75 ± 2.10	268.20 ± 9.59
8	ND	153.65 ± 7.78
12	ND	101.29 ± 5.34
24	ND	37.58 ± 3.45
48	ND	7.42 ± 0.68

All values reported are mean ± SEM, (n=6); ND: Not detected

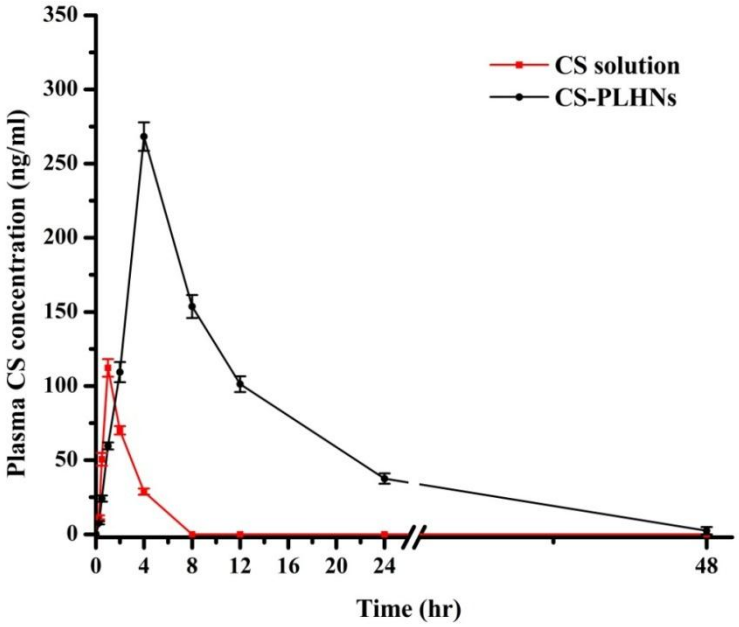

Figure 7.18 Plasma drug concentration time profile of CS-PLHNs and CS solution following single dose oral administration in rats; Dose: 20 mg/kg (vertical bars represent ± SEM; n=6)

The various pharmacokinetic parameters obtained by non-compartmental analysis are summarized in Table 7.15. The significant difference (p<0.05) was noticed in the pharmacokinetic parameters of CS solution and CS-PLHNs, after non-compartmental analysis of CS plasma concentration time profile. As can be seen from the mean plasma concentration–time curve, oral administration of CS solution resulted into faster appearance of CS in blood. The C_{max} of 268.20 $\pm$ 9.59 ng/ml was observed for CS-PLHNs after single dose administration, which was ~2.4 times higher than those obtained for the CS solution (112.23 $\pm$ 5.90 ng/ml). The hydrophobic surface as well as nano-size of the CS-PLHNs could have facilitated the permeation of CS across GIT, by virtue of their specific absorption mechanisms and that might be responsible for the higher value of C_{max} [27, 226]. The T_{max}, $T_{1/2}$ and MRT obtained with CS-PLHNs were significantly higher than those obtained with pure CS solution. The T_{max} was also 4 times delayed for CS-PLHNs as compared to CS solution, which confirmed the sustained *in-vivo* CS release potential of CS-PLHNs similar to the *in-vitro* release profile. The plasma level of CS from CS solution declined sharply after 1.52 $\pm$ 0.02 hr, indicating rapid systemic elimination of the CS owing to its poor plasma protein binding, which was further evident by its low systemic MRT of 2.79 $\pm$ 0.03 hr. Whereas, ~5.40 times and ~4.76 times enhanced $T_{1/2}$ and MRT, respectively was obtained with CS-PLHNs as compared to free CS solution. The plasma level of CS after the oral administration of CS-PLHNs detected up to 48 hr. It might be due to retention of CS-PLHNs in an intestinal mucosa, which extends the absorption and releases encapsulated CS over longer period of time thereby, reiterating the potential of CS-PLHNs as a sustained delivery system [106, 107, 235].

Table 7.15 Pharmacokinetic parameters of CS and CS-PLHNs following single dose oral administration in rats (Dose: 20 mg/kg)

Parameters	CS solution	CS-PLHNs
C_{max} ($ng.ml^{-1}$)	112.23 ± 5.90	268.20 ± 9.59*
T_{max} (hr)	1 (± 0)	4 (± 0)
AUC_{0-48h} ($ng.hr.ml^{-1}$)	232.16 ± 12.31	2748.82 ± 276.61*
$AUC_{0-\infty}$ ($ng.hr.ml^{-1}$)	295.53 ± 17.79	3033.81 ± 193.77*
$T_{1/2}$ (hr)	1.52 ± 0.02	8.22 ± 0.51*
MRT (hr)	2.79 ± 0.03	13.30 ± 0.59*
Fr	1	11.89 ± 1.25*

**significant values at $p<0.05$ compared with CS solution (Unpaired student t-test); All values reported are mean ± SEM, (n=6).*

Moreover, the values of AUC_{0-48hr} and $AUC_{0-\infty}$ for CS-PLHNs were also significantly improved ($p<0.05$) compared to pure CS solution, indicating the significant increase in the bioavailability of CS. From the various pharmacokinetic parameters, it was clear that CS-PLHNs have the promising potential for oral delivery of CS with approximately ~11.9 fold higher relative bioavailability, compared to pure CS solution, upon single oral dose administration. The significant improvement ($p<0.05$) in oral bioavailability of CS, achieved with CS-PLHNs might be resulted due to the nano-sized structure and increased surface area, which would have enhanced systemic absorption of CS-PLHNs through specialized absorption mechanisms across GIT such as paracellular transport, transcellular transport via enterocytes and M-cells of the PP [23, 106, 107, 236]. Furthermore, phospholipid covering over the polymeric core might have improved the bioadhesion of CS-PLHNs with the intestinal membrane and assisted in the CS-PLHNs movement through paracellular pathway [248, 249].

Results corroborate well with the findings of *ex-vivo* and *in-vivo* intestinal uptake studies and further substantiate the hypothesis.

7.2.3.8 *In-vivo* mast cell stabilizing activity

The degradation of the isolated peritoneal mast cells in different groups, after incubation with the compound 48/80 is depicted in Figure 7.19. The results of mast cell stabilizing activity in the rats are summarized in the Table 7.16.

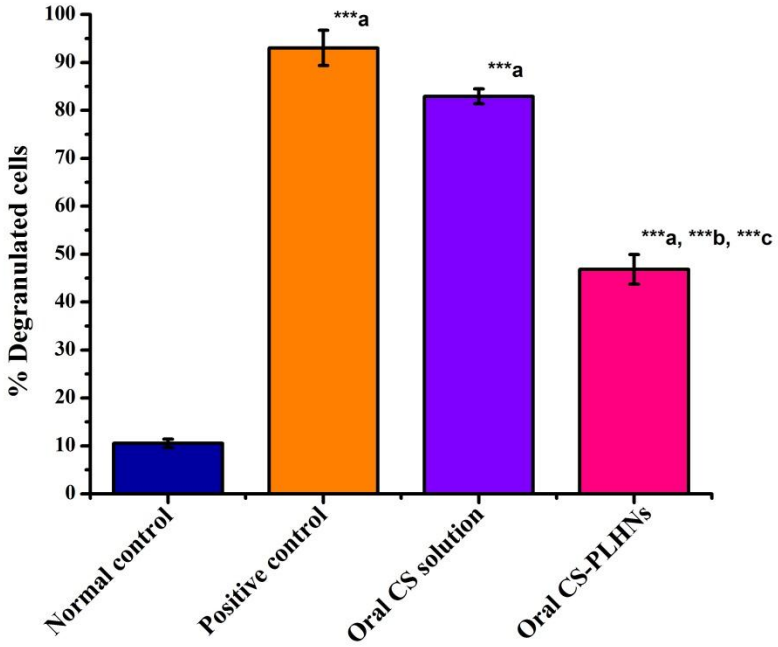

Figure 7.19 Effect of oral administration of CS solution and CS-PLHNs on degranulation of peritoneal mast cells in rats (Dose: 20 mg/kg); Vertical bars represent ± SEM; n=6.
***p<0.001; a *vs* normal control, b *vs* positive control and c *vs* oral CS solution; One-way ANOVA followed by Tukey's multiple comparison test**

In the normal control group, isolated peritoneal mast cells showed 10.515 ± 0.8813 % activation. Whereas, positive control group showed 93.033 ± 3.648 % activation of

mast cells, upon incubation with compound 48/80. Prophylactic treatment with oral administration of the CS solution (20 mg/kg) and CS-PLHNs (20 mg/kg on 1st, 3rd, 5th and 7th day) for 7 days in the rats has offered significantly higher (p<0.05) protection against mast cell degranulation and reduced the total number of activated mast cell. Oral administration of CS solution provided ~10.87 % protection against mast cell degranulation compared to positive control and showed 82.92 ± 1.558 % activation after incubation with compound 48/80. However, significantly much higher protection against mast cell degranulation was observed in case of CS-PLHNs as compared to CS solution (p<0.001).

Table 7.16 Effect of oral administration of CS solution and CS-PLHNs on compound 48/80 induced degranulation of peritoneal mast cells and histamine release in rats (Dose: 20mg/kg)

Treatment Groups	% degranulated cells	Histamine release (µg/ml)
Normal Control	10.515 ± 0.881	0.033 ± 0.0019
Positive Control	93.033 ± 3.648***[a]	0.190 ± 0.0083***[a]
Oral CS solution	82.920 ± 1.558***[a]	0.166 ± 0.0043***[a]
Oral CS-PLHNs	46.821 ± 3.1***[a],***[b],***[c]	0.097 ± 0.0085***[a],***[b],***[c]

*All values reported are mean ± SEM, (n=6). ***p<0.001; a vs normal control, b vs positive control and c vs oral CS solution; One-way ANOVA followed by Tukey's multiple comparison test.*

Oral administration of CS-PLHNs provided ~49.67 % protection against mast cell degranulation compared to positive control and showed 46.821 ± 3.1 % activation after incubation with compound 48/80. Additionally, lower amount of histamine release for CS-PLHNs treated group compared to CS solution treated and positive control group suggested the better efficacy of CS-PLHNs for stabilizing the mast cells

from compound 48/80 like allergen evoked degranulation [199-202]. The enhanced efficacy for CS-PLHNs compared to CS solution after oral administration indicated that CS-PLHNs would have delivered significantly higher amount of CS in the systemic circulation by improving its GIT permeability to CS solution and thereby, provided higher protection to the sensitized mast cells against degranulation, which in turn strengthens the findings of *in-vivo* pharmacokinetic study.

7.3 Summary

The present strategy provides a deep insight into the captivating features of PLHNs for oral delivery of CS like poorly permeable hydrophilic drug molecule. The CS-PLHNs were successfully developed by double emulsification solvent evaporation method ($W_1/O/W_2$) with little modifications. As CS is a highly hydrophilic drug, its encapsulation inside the nanoparticles was a challenge. The Plackett-Burman screening design was used for preliminary screening of large number of variables in order to identify critical variables affecting the formulation characteristics of CS-PLHNs. A 3-level, 4-factor Box-Behnken experimental design was imperatively enforced to optimize and to understand the combined influence of screened critical variables (i.e., lipid/polymer ratio, concentration of surfactant, organic phase/aqueous phase ratio and concentration of polymer) on physicochemical properties of CS-PLHNs, i.e., particle size, EE and PDI. The quality by design approach suggested that Box-Behnken experimental design provided a high degree of prediction and realization for optimization of the physicochemical properties of CS-PLHNs by controlling the different formulation variables. The optimized CS-PLHNs showed particle size of 227 $\pm$ 3.8 nm, EE of 57.8 $\pm$ 1.32 % and PDI of 0.151 $\pm$ 0.027. The optimized batch has desirability of 0.866. The solid state characterizations of optimized CS-PLHNs suggested the encapsulation of CS in an amorphous form inside

the matrix of PLHNs without any physical as well as chemical interactions. The morphological studies pointed towards the existence of smooth, spherical shaped, core-shell architecture of CS-PLHNs. *In-vitro* release study of CS-PLHNs in phosphate buffer pH 7.4 showed extended release up to 48 hr by diffusion controlled process. The optimized CS-PLHNs exhibited remarkable stability at different environmental conditions over the period of 6 months, stored at room temperature (25 $\pm$ 2 ^{o}C), refrigerated condition (4 $\pm$ 1 ^{o}C). *Ex-vivo* intestinal permeation study demonstrated ~5.98 fold improvements in CS permeation across the intestinal barrier by forming CS-PLHNs as compared to pure CS solution. Further, *in-vivo* intestinal uptake study performed using confocal microscopy following oral administration confirmed the permeation potential of CS-PLHNs, as indicated by their strong green colored fluorescence. *In-vivo* bioavailability and pharmacokinetic study was performed in rats and revealed ~11.9 fold enhancements in oral bioavailability of CS after its incorporation into PLHNs as compared to pure CS, which ought to be the lipophilicity imparted by PLHNs. Eventually, *in-vivo* mast cell stabilizing activity performed in rats demonstrated significant protection against mast cell degranulation with oral administration of CS-PLHNs than free CS solution. Conclusively, the developed CS-PLHNs could definitely be considered as promising delivery strategy for altering the existing oral pharmacotherapy of CS as a result of its improved oral bioavailability with greater efficacy.